Durability Analysis of Helical Coil Spring in Vehicle Suspension Systems

Dhananjay Kumar

Thesis submitted to the Faculty of the

Virginia Polytechnic Institute and State University

in partial fulfillment of the requirements for the degree of

Master of Science

in

Engineering Mechanics

Surot Thangjitham, Co-chair

Robert L. West, Co-chair

Mark S. Cramer

August 13, 2021

Blacksburg, Virginia

Keywords: Helical Coil Spring, Suspension System, Road Surface Roughness,

Linear System, Vibration, Finite Element Method, Modal Analysis,

Frequency Response Analysis, Stress-Life Approach, Durability, Fatigue Life.

Durability Analysis of Helical Coil Spring in Vehicle Suspension Systems

Dhananjay Kumar

ABSTRACT

The suspension system in vehicles supports the vehicle's road stability and ride quality by scaling down the vibration responses resulting from road surface's roughness. This research focuses on fatigue life analysis of coil spring component. Static linear analysis is conducted on the 3D model of helical coil spring to investigate deformation and stress responses. Modal analysis evaluates the characteristics of vibration, i.e. natural resonance frequencies and corresponding mode shapes. The stress frequency response is generated after performing the harmonic analysis on the spring. Dynamics and performance of spring are analyzed over practical frequency range of 0 Hz to 200 Hz. Fatigue life estimation of vehicle suspension spring is performed using the stress data obtained from frequency response analysis. The stress-life (S-N) approach is utilized for fatigue life assessment of suspension spring. This durability analysis technique can be utilized in the automotive industry to improve reliability of vehicles. The outcome of this research can contribute in analysis and design of modern smart vehicles.

Durability Analysis of Helical Coil Spring in Vehicle Suspension Systems

Dhananjay Kumar

GENERAL AUDIENCE ABSTRACT

The suspension system in vehicles supports the vehicle's road stability and ride quality by scaling down the vibration responses resulting from road surface's roughness. This research focuses on the fatigue life analysis of suspension spring component. Initial phase of analysis is conducted to investigate the deformation and stress in 3D model of spring. Dynamics and performance of spring are analyzed over applicable frequency range of 0 Hz to 200 Hz. Fatigue life of vehicle suspension spring is evaluated using stress data from frequency response analysis. This durability analysis technique can be utilized in the automotive industry to improve reliability of vehicles. The outcome of this research can contribute in analysis and design of modern smart vehicles.

Acknowledgments

Author would like to express sincere gratitude to the graduate advisory committee comprising of Prof. Surot Thangjitham, Prof. Robert L. West, and Prof. Mark S. Cramer for the valuable guidance, mentoring, and encouragement throughout the course of this research.

Also, author expresses special appreciation to Prof. Robert L. West for providing continuous support by accepting the Co-chair position in the advisory committee. Author is thankful to Dr. Yat Sheng Kong, and all post graduate students, faculty and staff of the Engineering Science and Mechanics Department at Virginia Tech.

Author wants to thank the parents, family members, and friends for their love, patience, and continuous encouragement. Importantly, author would like to extend the heartfelt gratitude to the administrative staff of graduate school at Virginia Tech, for the guidance and support throughout the duration of research.

Contents

List of Figures

List of Tables

List of Abbreviations

ϵ-N Strain-life

ν Poisson's ratio

ρ Density

E Modulus of elasticity

S-N Stress-life

3D   3 dimensional

ANN   Artificial neural network

ASTM   American society for testing and materials

BS   British standards

CAD   Computer aided design

CAE   Computer aided engineering

CAL   Constant amplitude loading

DIN   Deutsches institut für normung

DOF   Degree of freedom

FE   Finite element

FEA   Finite element analysis

FEM   Finite element modeling

FRF   Frequency response function

HCF   High cycle fatigue

HMLP Hybrid multi-layer perceptron

LCF   Low cycle fatigue

MBD Multi-body dynamics

MLR Multiple linear regression

OL   Overload

PSD   Power spectra density

R   Stress ratio

SAE   Society of automotive engineers

UL   Underload

VAL   Variable amplitude loading

Chapter 1

INTRODUCTION

1.1 An Overview: Evaluation of Fatigue Life

Automotive components are exposed to vibration conditions and are subjected to various dynamic loadings, during the operating conditions. Loadings and vibrations induce stress in the components that can lead to mechanical failure. Mechanical failures have been the foundation for injuries and loss of assets. Mechanical failures in the automotive components can be diminished rather than completely eradicated. Many mechanical structures and components have effectively reduced the mechanical failure by following adequate design procedures, e.g. turbines [1], automotive dampers [2] and aircraft [3]. Continuous vibration loading can have either constant or varying amplitudes that originates cracks, deprivation in ductility of material and leading to failure of mechanical component [4]. This type of failure is termed as fatigue failure. In practical applications, mechanical components and structures are exposed to varying amplitudes load scenarios where stress-strain cycles are oscillating with time [5, 6].

Fatigue contributes to at-least 50 percent of the failures of mechanical components and structures [4, 7]. Fatigue failure can lead to fatal accidents involving risking multiple lives. Hence, analysis of fatigue behaviour becomes a crucial part in the mechanical design of enhanced durable product. The stress-life (S-N) curve was first introduced in 1850 by a

German engineer, August Wöhler, to study and investigate fatigue behaviour of materials. Wöhler conducted the study using specimens of cylindrical geometry and under constant amplitude loadings. The *S-N* curve has significantly contributed in the understanding of fatigue properties of materials [8].

1.2 Durability of Vehicle Suspension System

Manufacturing process and product design are two factors that impact the durability of an automobile component. Most mechanical automotive components were subjected to heat treatment or process of shot peening to increase the fatigue life prior deploying components for mechanical operations [9]. Being a complex dynamical system, the vehicle response is influenced by the rapid change of contact between tires and road surface. Dynamic vibrations are generated in vehicle components by unsteady interactions, which can further lead to failure of components. During the design stage of automobile components, appropriate manufacturing process must be taken into consideration to deal with fatigue failure induced by unpredictable vibrations [10, 11].

Vibrations are induced in an automobile via running engine, drivetrain and road excitations [12]. Fatigue failure of vehicle component is critically influenced by road induced vibrations [13]. Thus, suspension system was setup in automotive vehicles to isolate the road disturbances and improve the ride comfort, also to increase the reliability of other supporting vehicle components. At large, a set of spring dampers are present in suspension system that bear the vehicle weight and permit the vertical translation motion of wheels. Tire also constitutes in the suspension system, regular replacement are necessary as they are considered as a wear and tear component [14]. Consistent examination of tire bring out

more attentiveness towards the fatigue analysis of spring because the spring is supposed to be deployed in vehicle until its targeted durability warranty period ends i.e. for a maximum of 6 years [15].

When a vehicle passes through a rough terrain, the vibration energy is absorbed by the compression and expansion motion of the coil spring. The spring reacts interactively to the road conditions. Helical spring has circular geometry; the principal stresses are observed in different directions during the compression stage. The process of fatigue analysis is complex because of the complicated stress conditions observed in the coil spring. A study was performed to assess profile of road based on a new technique of vehicle ride and durability [16]. During the research, it was identified that both vehicle characteristics of durability and ride were predominantly influenced by excitation of road surface.

A research was performed on 1400 springs to analyse the fatigue characteristics of coil spring [17]. Fatigue testing machine was used in experimental testing to investigate influence of spring material state and wire diameter on fatigue life of coil spring. Being destructive testing, all the springs were destroyed in the experiment. The fatigue testing experiment was not cost efficient. However, to understand the behaviour of helical coil spring and failure resulting from fatigue, numerical analysis using finite element modeling (FEM) is a cost effective and reliable solution [18].

Road excitation influences the ride quality, and also contributes to the fatigue of suspension coil spring. Rough road conditions can affect the passenger comfort during the vehicle ride. The design of vehicle suspension system is optimized to counteract the effect of vibrations induced by various road conditions [19]. The experiment setup was developed having a quarter car model to replicate the vehicle ride conditions. Combination of various spring stiffness and damping coefficient values generated vertical acceleration amplitudes of

vehicle, that effectively evaluated the optimized parameter. A technique was proposed to refine the quarter model of vehicle suspension for ride analysis [20]. The method resulted in a simplified equation to evaluate the damping impact in vehicle ride comfort.

1.3   Problem Statement

In the present age, there is demand and requirement for passenger vehicle having durable system and excellent riding properties. Therefore, good suspension design can serve the purpose of automotive industries to satisfy the consumer needs and sustain in the competitive automotive world. However, the design process of vehicle suspension spring consumes a good amount of time focusing on selection of suitable vehicle target level, hard points, system architecture, bushing rates, spring rates, analysis of loading on suspension, characteristics of shock absorber, each component's structural integrity and vehicle dynamics assessment of the design results [21]. These tasks require extensive human efforts, resources and time to validate the suspension spring design of sustaining the repetitive road induced disturbances without early stage failure and providing smooth vehicle ride attributes.

Vibrations contribute to a greater extent in the ride performance of automobiles [22]. Recent literature draws attention towards the potential irrelevancy arising from independent analyses on durability and vibrations of the vehicle suspension. After executing integrated suspension structural analysis, suspension design contribution towards the ride dynamics of vehicle were examined for betterment in vehicle ride characteristics. Hydro mounts were utilised in vehicle simulation model for extracting durability loadings for ride and durability study of vehicle [23]. The suggested technique had limitations of complicated modelling and each tuning on suspension generated new transfer function. The repetition

of procedures were required for setting up a balance between fatigue strength of suspension components and vehicle ride characteristics for obtaining design optimization. The iterative time consuming procedure, generated minute engineering value. Essentially, there exists good probability of error or unavailability in the simulation or measurement that could possibly generate obstruction in analyzing desired results [24]. In the adverse scenario, it could hinder the timeline of product launch and impact the reputation and stature of the automotive industry.

It becomes quite important to perform design analysis quickly by opting a robust and simple technique which could serve as a guideline in reducing the repetitive human efforts. Data obtained form durability tests performed on old vehicles were not utilized for future vehicles after investment of human efforts and monetary funds. The need that arises is to have a workflow to use the information from present generation of vehicles to the upcoming new vehicle generation which reduces the unnecessary repetition of development processes. This research focuses on providing solution to the requirement of automotive industry in present era. However, extensive road load analysis had been performed, vehicle ride dynamics although being closely associated to the suspension components were not considered of the integrated structure of the analysis. This leads to need for determination of relationship existing between vehicle ride comfort and durability of suspension for assistance during automobile design.

1.4 Research Objectives

This current study aims to establish the relationship of vehicle spring durability for vibration along with considering the varying profiles of road terrain. Several objectives have been

determined for the successful execution of this study. The specific objectives are

1. Generation of helical coil spring model in 3D CAD software, and using FEA software tool to obtain the mean stress about static equilibrium position from static linear analysis of spring CAD model.

2. Performing the modal and frequency response analyses on the helical spring model to estimate the natural resonance frequencies of vibration, and obtaining the stress frequency response data over practical frequency range of 0 Hz to 200 Hz.

3. Determination of durability relationship, predicting the vehicle vibration by analyzing the simulation of a quarter vehicle model traveling on wavy road surface.

4. Establishing the prediction of fatigue life in helical suspension spring, considering the mean stress, σ_m, and using the *S-N* approach.

1.5   Significance of Research

This research comes up with innovative approach of durability analysis of suspension spring and it contributes new approach to the fields of vehicle dynamics, mechanical design and durability. This study performed on the coil spring focuses on developing a technique for durability assessment of vehicle vibrations. Initially, the stress was analyzed for realistic prediction of suspension spring fatigue life. Later, durability evaluation was performed on automotive coil spring for varying wavy road conditions. It becomes crucial to qualitative gauge the suspension spring design in refining the road excitations.

Furthermore, this research constructs a relationship between vehicle suspension spring and vehicle ride dynamics. In application process, designing a suspension spring

having both vibration properties, and good durability consumes good amount of time and efforts. Hence, assessment of durability and vehicle ride characteristics becomes important to reduce the required time. The relationship developed under this study is quite robust, and the results could be extracted instantly within acceptable range of accuracy which is important contribution from this current research.

Chapter 2

LITERATURE REVIEW

2.1 Automobile Suspension

Automotive suspension systems have been continuously developed over the years. All types of suspension systems have undergone through consistent development cycles. The vehicle suspension systems are classified in three categories namely active, passive and semi-active suspensions. An active type comprises of spring and damper that dissipates or gain energy into the system in compliant manner whereas the variable damping with predefined characteristics of spring is allowed in a semi-active suspension system. Passive suspension system includes a damper and pair of springs having predetermined characteristics. Passive system being the simplest, it is most extensively accepted in automotive applications [25]. Further there are advanced suspension systems, the suspension system having continuous varying damping, while air springs with variable spring and damper characteristics utilised by the automotive companies [26].

Passive suspension systems can be broadly categorised in further three groups namely dependent, independent and semi-dependent systems. Hotchkis suspension system is one of the most popular example of dependent suspensions as shown in Fig. 2.1. Motion of the left and right wheels are dependent on each other as both the wheels are connected to same solid axle. If any wheel of dependent suspension moves over an uneven surface, subse-

quently vibrations are originated in other wheel. This category of passive suspension system has capability to insure a fixed camber which is appropriate for heavy duty automobiles. In semi-dependent suspension, a compliant link replaces the rigid connection between both the wheels. Trailing twist axle suspension is an example of semi-dependent system. The dependent and semi-dependent system can be mainly differentiated based on the count of compliant links attached to both the left and right wheels.
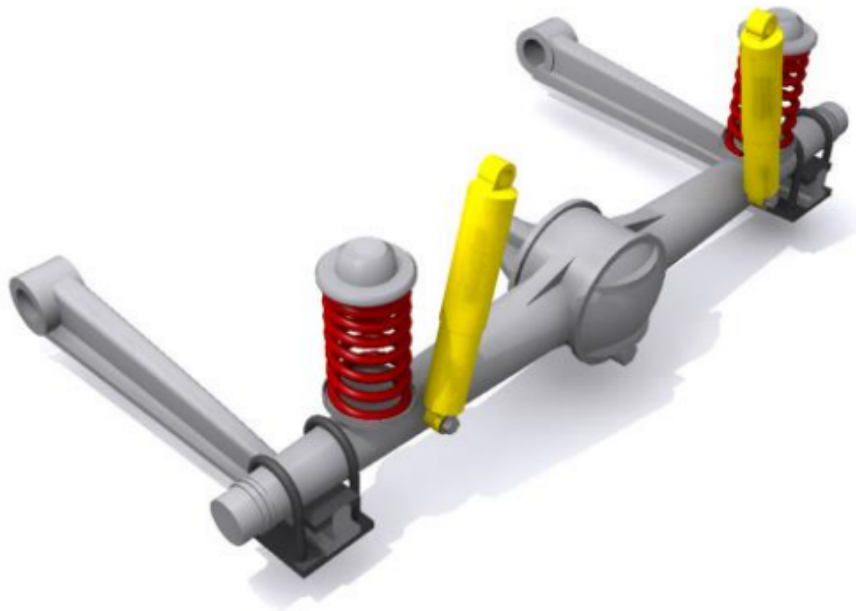
Figure 2.1: Dependent System: Hotchkis Suspension.
Source: Jazar [27]

The two wheels in independent suspension system that are mounted on vehicle axle can move independently. In contrast to dependent suspension system, this class of suspension system is advantageous while packaging and allows greater freedom in design. The Macpherson strut, multilink, double wishbone, and trailing arm are few common examples of independent suspension system as described in Fig. 2.2. The Macpherson strut as shown in Fig. 2.2 (a), has a strut combined with spring and shock absorber and it connects wheel

with vehicle frame. This suspension system has lesser components and acknowledged for being lightweight, cheaper and compact in size [28].
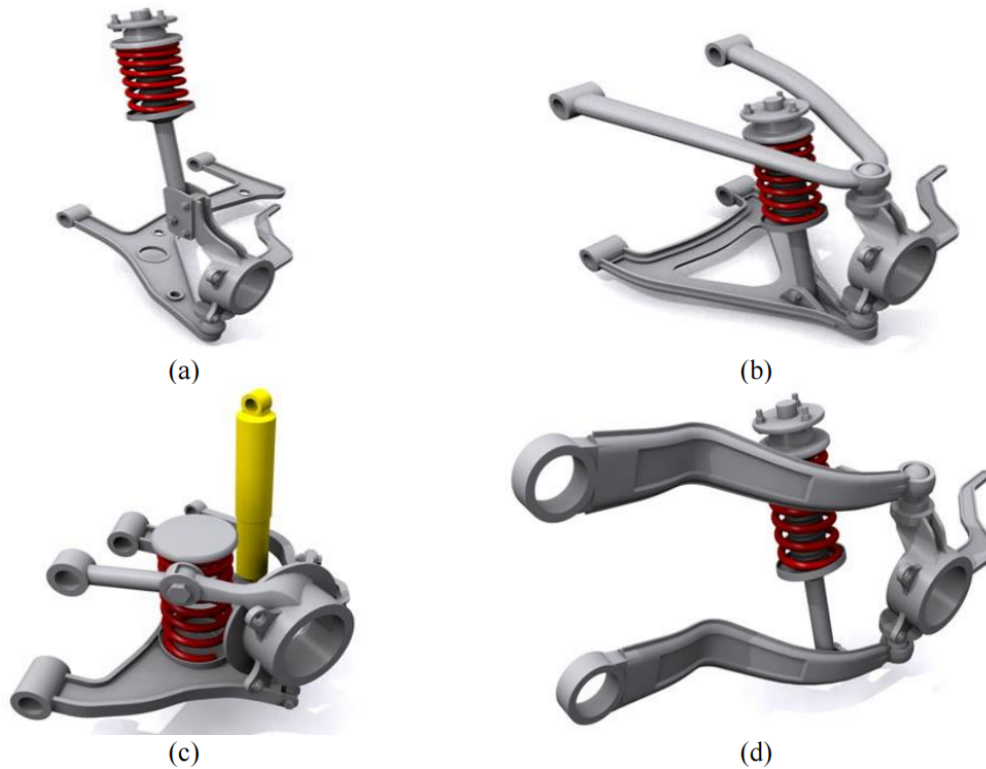
Figure 2.2: Types of Independent Suspension System.
Source: Jazar [27]

The other two categories of independent systems, double wishbone and multilink systems have better performance and versatility than Macpherson system. Double wishbone system as shown in Fig. 2.2 (b), generally comprises of two lateral control arms of unequal lengths accompanying with coil spring and shock absorber. Whereas the multilink system has five connecting links as described in Fig. 2.2 (c). Design parameters increase with the increase in number of connecting points in suspension system and it evokes the kinematic and dynamic complexity in the suspension system which is good for vehicle handling [29].

However, the cost may rise with increase in number of links and components.

Trailing arm suspension system is commonly applied by attaching pivot point to the axle as shown in Fig. 2.2 (d) and extensively applied in heavy duty vehicle having solid axle such as military trucks [30]. Type of vehicle, allocated cost and desired performance are the deciding parameters in choosing the appropriate vehicle suspension system. During vehicle design, in-depth understanding of suspension mechanism is required for selecting suitable suspension system.

2.2 Mechanism of Suspension Components

Suspension system mechanism describes the kinematics of wheel's movement in lateral and vertical directions while vehicle is moving on the road. The wheels move vertically upward and downward when the vehicle travels through various terrains and rough road conditions as shown below:
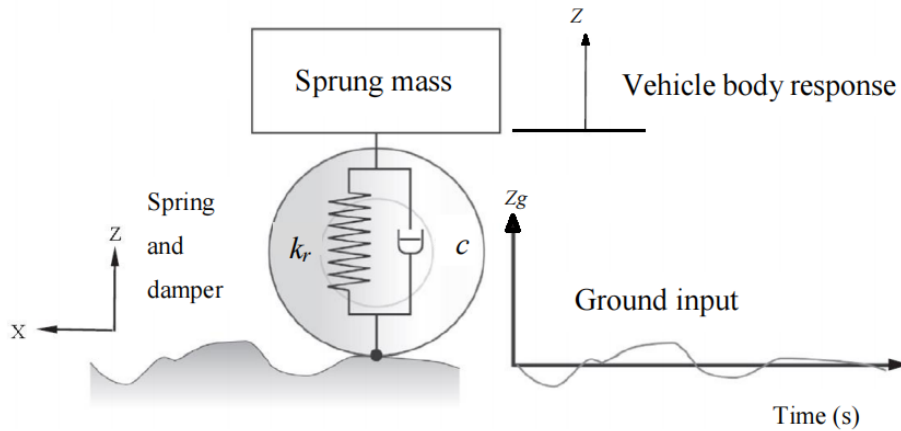
Figure 2.3: Quarter Car Model.
Source: Blundell and Harty [31]

here Z_g is excitation of road surface, Z is vehicle response to excitation, c is damping coefficient of the damper, and k_r represents ride rate as described by Eq. 2.1. Wheels move in perpendicular direction to the road surface that expands and compresses the spring

component of vehicle suspension system. The energy is absorbed by the spring and it is released moderately. Remaining load that gets transmitted to body of the vehicle creates dynamic body response. Most vehicle suspension system apply this mechanism to reduce the disturbances induced by the road surface.

While the vehicle is in motion, both coil spring and wheel displace relative to each other. Motion ratio (MR) creates relationship between displacements of suspension spring and wheel [32]. It is proposed to have MR value as 1 to ensure vehicle balance during roll of front suspension system [33]. While modelling, tire element is considered as linear spring which is in series connection with coil spring, and ride rate, k_r, is expressed as

$$k_r = \frac{k_s k_t}{(k_s + k_t)} \tag{2.1}$$

here k_s is spring rate or spring stiffness, and k_t is tire stiffness. The compression and extension mechanism of helical coil spring is shown below:
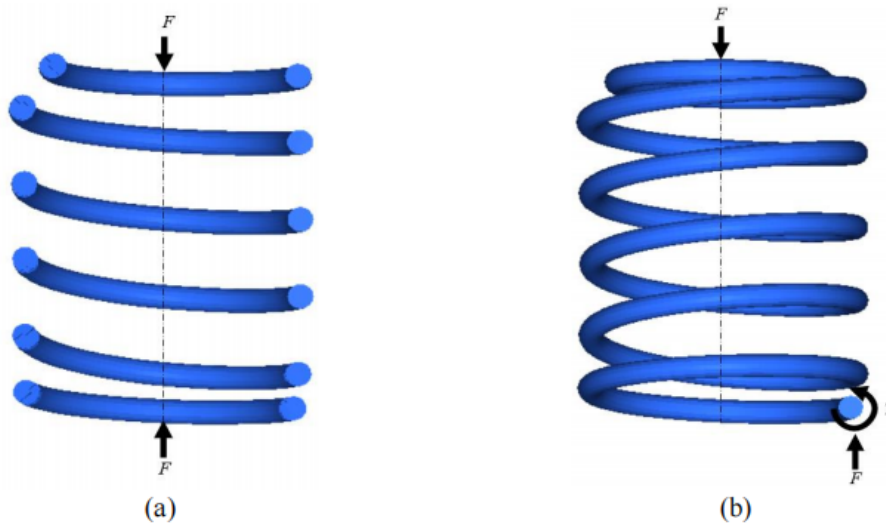
Figure 2.4: Spring Loading Diagram: (a) Uni-Axial Loading, (b) Free Body Diagram. Source: Sequeira et al [34]

12

When vertical applied force, F, is applied on the coil spring, it gets compressed and is subjected to torsional shear, T, as described in Fig. 2.4 (b). The fundamental Hooke's law is applicable for coil spring, that can be stated by the Eq. 2.2 [35]. Hooke's law has been existing for more than three centuries and is extensively referred during the design of coil spring [36].

$$K = \frac{F}{x} \tag{2.2}$$

here K and x represent stiffness and displacement of spring respectively. The stiffness of spring, K, also known as spring rate or spring constant or spring scale, is obtained from the slope of force-deflection curve. This constant can behave in linear or nonlinear manner.

Spring deform with application of load and the objective of extension and compression movement of spring is to attain equilibrium by returning the attached mass to its initial static position. In case of unanticipated impact, the rebound and vibration in coil spring lasts until the entire energy transmitted from the impact gets exhausted. Only spring component in the vehicle suspension system cannot provide smooth ride to the passengers. Shock absorbers are installed in suspension system to diminish the vibrations induced in the helical spring by converting kinetic energy to heat which gets dissipated using hydraulic fluid [37]. The viscous effects are commonly observed in damping behaviour of the shock absorber. There is a relation between viscous damping of shock absorber and the velocity of excitation, $\dot{x}$, which is expressed below:

$$c = \frac{F}{\dot{x}} \tag{2.3}$$

here c is damping coefficient. Rebound and compression are two mechanisms observed in a shock absorber as described below in Fig. 2.5 (a) and (b) respectively. Mechanism of

damper has been expressed by the damping curve as shown in Fig. 2.5 (c).

(a)   (b)

(c)
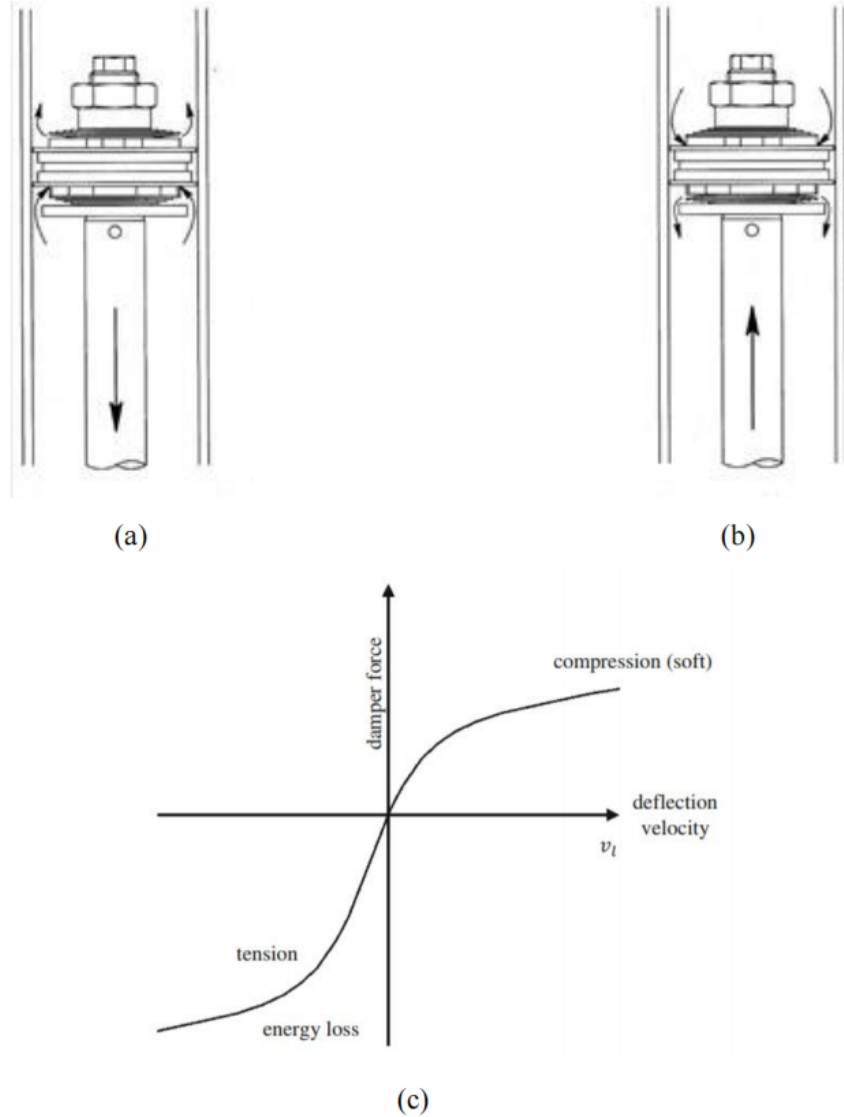
Figure 2.5: Damper Mechanism.
Source: Schramm et al [38]

The hysteresis effects observed in the curve is owing to the oil being compressed by the valve [39]. Compression represents positive damper force whereas negative damping force indicates rebound state of the damper [38].

When the focus is on dynamic properties of vehicle, tire is also considered a sig-

nificant component of the suspension system. Knowing the tire properties is essential in order to replicate the vehicle ride properties. The stiffness and damping values are needed to simulate the ride scenario of automobile. The tire is commonly modelled as linear system of spring and damper as shown in Fig. 2.6, where k_t is stiffness of tire, c_t is tire damping coefficient, m_t is mass of wheel, δ_z is vertical displacement of tire, Z_{SAE} is vertical axis as per SAE coordinate system, and X_{SAE} is the longitudinal axis.
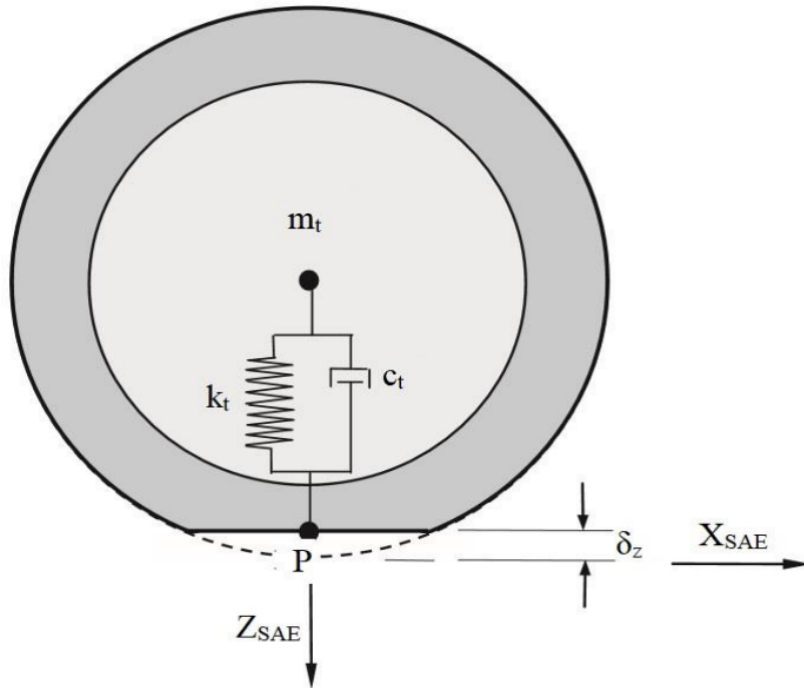
Figure 2.6: Automotive Tire Model.
Source: Blundell and Harty [31]

The tire is moderately damped in passenger cars and vehicles in motion are normally influenced by wheel hop [31]. A linear tire model system is perfectly adequate in simulating majority of automotive passenger vehicles [40]. In case of heavy vehicles, the nonlinear tire model should be considered over linear tire model in consequence of the large deflection. The Kelvin-Voigt-type model, and Maxwell model are two ways to model the

suspension tire. The Kelvin-Voigt-type model is represented by parallel connection of a Newtonian damper and Hookean elastic spring, whereas the Maxwell model comprises of a series connected viscous damper and elastic spring.

The movement of wheel is guided by control arm and it is an important component that regulates stability of vehicle and ride comfort [41]. The mounting of control arm is in between vehicle chassis and vertical suspension sustaining the wheel. It is connected to the chassis by one pivot bushing which directs the location of control arm end in one DOF and maintains distance in radial direction from inboard. While moving along rough road terrain, lower arm oscillates in constant radius and drives wheel's motion along an arc. The weight of control arm has influenced few advancements in the field of vehicle dynamics. Design enhancement of reinforcing carbon fiber on the composite was suggested to lower down the weight of suspension while sustaining its strength [42].

Components of suspension usually have the same objective for majority of automotive passenger vehicles. Although, varying the setup of suspension components modifies the dynamic attributes of the vehicle. The Macpherson and double wishbone systems are the most commending suspension systems and they are listed in specifications of numerous automotive vehicles [43]. The high performance car manufacturing companies have deployed the Macpherson suspension system [28]. Meantime, many car manufactures installed the Macpherson system as the front suspension system of vehicle. Therefore, researches have been conducted for simulating and analyzing the Macpherson suspension system and vehicle dynamics [44].

2.3 Coil Spring Parameters

Springs are flexible components used for storing energy and exerting force or torque. In case of door closers, springs are installed to generate torque. The nature of spring-force can be tensile or compressive, and direction can be radial or linear. Energy transfer is observed and spring energy is stored during the process of spring displacement. The stored spring energy gets released after the applied force producing the deflection of spring is removed. Classification of springs are based on the direction and characteristics of exerted force while the springs get displaced from equilibrium position. Various classes of springs are described below in accordance with nature of applied torque or force [45].

Table 2.1: Springs Classification Based on Force or Torque Nature.

Actuation	Spring type
Compressive	Helical compression
Compressive	Belleville
Compressive	Flat; e.g. leaf springs
Tensile	Helical extension
Tensile	Drawbar
Tensile	Constant force
Tensile	Flat; e.g. cantilever springs
Radial	Garter
Radial	Elastomeric bands
Radial	Spring clamps
Torque	Torsion
Torque	Power

Helical compression spring being the most common type of spring has constant round wire diameter and constant value of pitch. Configurations having variable pitch, barrel shape, hour glass shape and conical shape are also possible as shown in Fig. 2.7.
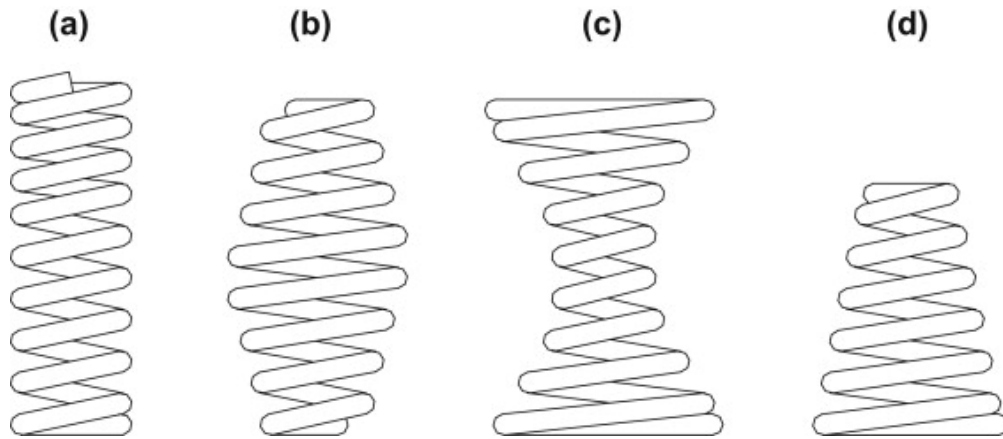
Figure 2.7: Helical Spring Configurations.
Source: Childs [45]

Other than diameter and pitch of coil spring, end treatments as shown in Fig. 2.8 are also crucial as it adds to the production cost and effect the performance of spring. The ends of spring are formed to improvise the interconnection between mating components of the suspension system.
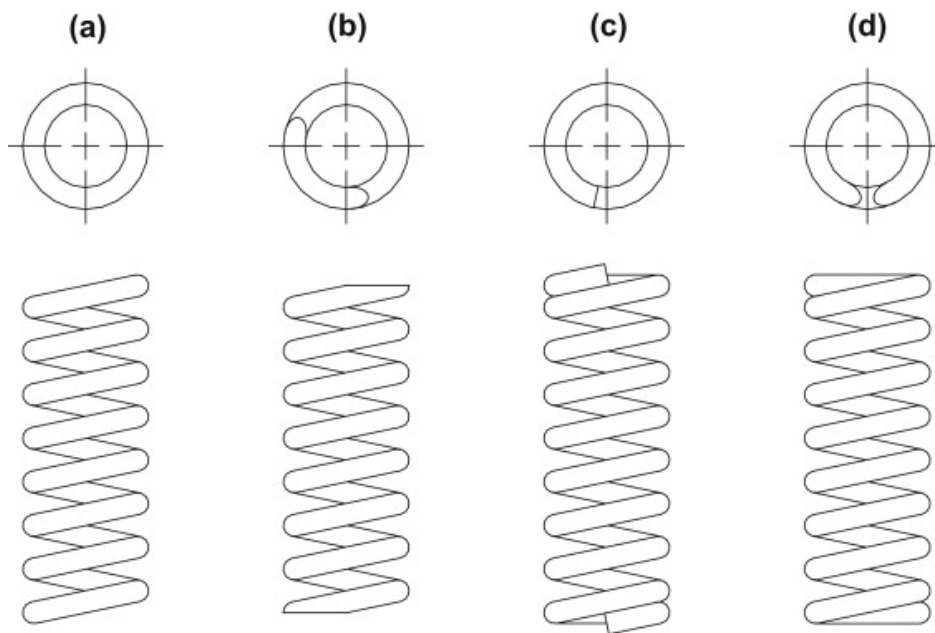
Figure 2.8: End Treatments: Plain, Plain Ground, Squared, and Squared Ground.
Source: Childs [45]

For coil springs having end treatments, it becomes important to account for the inactive coils and only active coils should be considered for evaluating the deflection and stresses from static structural analysis. The relationship between inactive and active coils for various end treatments can be obtained as shown in Table 2.2 [45], where N_a is active coils count, and N is total coils count in helical spring.

Table 2.2: Counting Number of Active Coils.

Plain/Open	Plain Ground	Squared	Squared Ground
$N_a = N$	$N_a = N - 1$	$N_a = N - 2$	$N_a = N - 2$

The principal geometrical parameters for a helical compression spring having constant pitch are described in Fig. 2.9. The wire diameter, mean coil diameter, freelength, and either the pitch or total number of coils define the geometry of helical coil spring and are
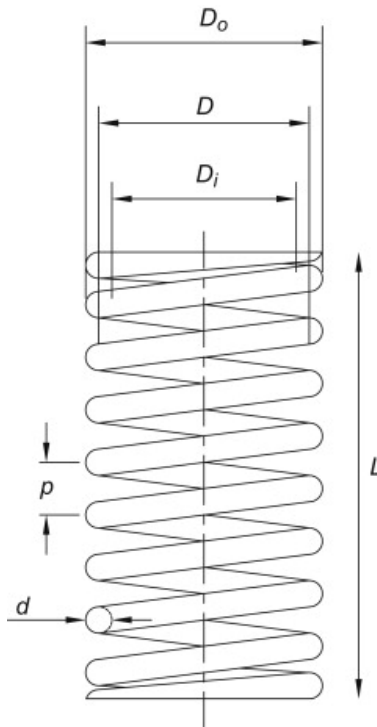
Figure 2.9: Dimensional Parameters.
Source: Childs [45]

19

used for corresponding analysis. The outer coil diameter, D_o, and inner coil diameter, D_i, are utilized in design of locating and mating associated components of vehicle suspension system. Other than the principal dimensions for an unloaded spring as identified above in Fig. 2.9, various lengths are defined for a coil spring as described in Fig. 2.10. The installed length, L_a, is obtained after the spring has been installed considering the primary deflection, $\delta_{initial}$. The operating length, L_m, is shortest compressed length of spring associated with the maximum working load. The solid length or shut height, L_s, is the shortest possible length when the adjacent coils are actually touching each other.
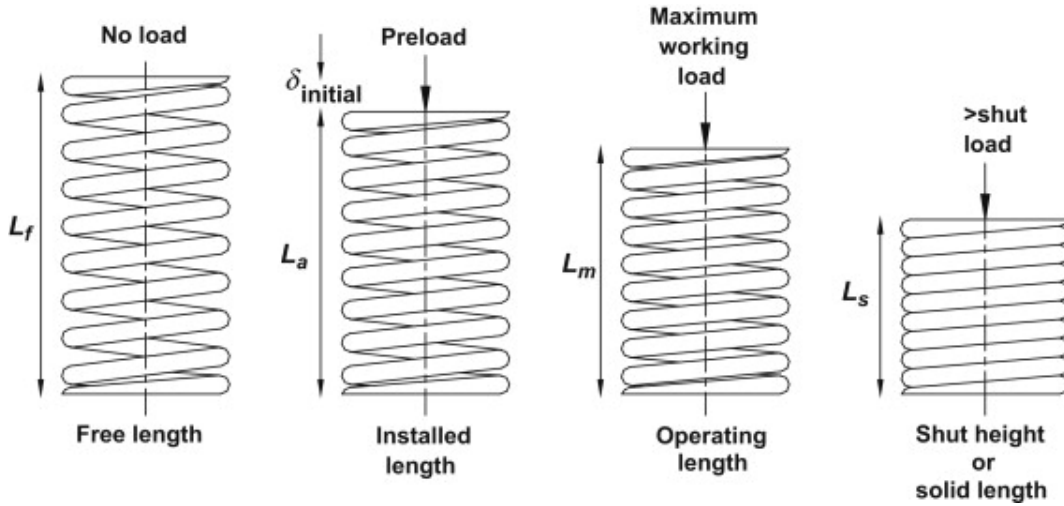
Figure 2.10: Various Spring Lengths Terminology.
Source: Childs [45]

Coil spring is installed in both Macpherson and double wishbone suspension systems primarily to diminish the vibrational impact in vehicle. Design of helical coil spring usually depends on the stiffness target value associated with natural frequency of vehicle suspension system. The force mean and amplitude loadings (F_m, F_a) are defined using the mathematical equations as mentioned below:

$$F_m = \frac{1}{2}\left(F_{max} + F_{min}\right) \tag{2.4}$$

20

$$F_a = \frac{1}{2} \left(F_{max} - F_{min} \right) \tag{2.5}$$

here F_{max} and F_{min} are maximum and minimum forces applicable on spring during vehicle in motion. Helical coil springs can fail either by fatigue in case of dynamic loading or by yielding caused by high stress in case of static loading. For evaluating helical spring geometry to overcome or estimate such failure, consideration of loading induced stresses in spring becomes necessary. The mean and amplitude shear stresses (τ_m, τ_a) are obtained using expressions as mentioned below:

$$\tau_m = K_s \left(\frac{8F_m D}{\pi d^3} \right) \tag{2.6}$$

$$\tau_a = W_{wahl} \left(\frac{8F_a D}{\pi d^3} \right) \tag{2.7}$$

here K_s is direct shear factor and W_{wahl} is the Wahl factor, and these two constant values can be evaluated using Eq. 2.8 and Eq. 2.9 as mentioned below [46]. The direct shear factor, K_s, accounts for direct shear stress effects while the Wahl factor, W_{wahl}, considers both direct effects of shear stress and the stress concentration factor arising from the curvature of helical spring component. Equation 2.6 is used for modelling of spring considering only static loading, and Eq. 2.7 is quite commonly utilised for fatigue modeling.

$$K_s = 1 + \left(\frac{1}{2C} \right) \tag{2.8}$$

$$W_{wahl} = \left(\frac{4C - 1}{4C - 4} \right) + \frac{0.615}{C} \tag{2.9}$$

21

here C describes spring index, and is defined as

$$C = \frac{D}{d} \qquad (2.10)$$

The value of spring index is preferred in a range between 4 to 12. Manufacturing of spring is difficult for value less than four and springs are prone enough to buckling for value greater than 12 [45].

Distribution of stress in helical springs is crucial for validation of design. Virtually, springs can be manufactured using any material. However, material having high ultimate strength, high yield point, and Young's modulus on lower side would be ideal one providing maximum energy storage while oscillatory motion of the helical spring. Spring manufacturing industries have largely adopted the techniques to analyze the stress distribution in coil springs. For stress analysis, FEA technique works satisfactorily for various types of coil springs [47]. FEA method was applied for validation of stress levels in different configurations of coil springs [48]. The relationship possessing by stress and strain have linear behavior, acknowledged as Hooke's law as described by Eq. 2.11, exists under certain assumptions and is followed by material within limit of elasticity.

$$\sigma = E\epsilon \qquad (2.11)$$

here σ represents stress, E is modulus of elasticity, and ϵ represents strain. Under linear elastic condition, the spring can restore the initial position from deformed configuration post removal of load.

Design of component may not be linear and does not follow the limit of elasticity, this scenario can be treated as plastic design application e.g. vehicle body requiring a non-

linear relationship between stress and strain [49]. In 1943, a mathematical relationship was proposed by W. Ramberg and W.R. Osgood to express the non-linear behavior of stress and strain. The initial representation of Ramberg-Osgood equation can be described as

$$\epsilon = \frac{\sigma}{E} + \left(\frac{\sigma}{K'}\right)^{\frac{1}{n'}} \tag{2.12}$$

here K' and n' describe cyclic strain coefficient, and cyclic strain hardening exponent. The former part of equation illustrates stress-strain elastic behavior, and later part defines plastic relationship of material. The Masing's model evaluates the incremental reversals associated with reference turning point as mentioned below [50]:

$$\Delta\epsilon = \frac{\Delta\sigma}{E} + 2\left(\frac{\Delta\sigma}{2K'}\right)^{n'} \tag{2.13}$$

here $\Delta\epsilon$ and $\Delta\sigma$ represent strain range and stress range respectively.

The strain hardening effect caused failure of many vehicle components due to accumulation of damage under plastic limits [51]. The transition effect of elastic to plastic behavior described as yield. For analyzing the simple stress state, especially for brittle materials, the principal stress theory was applied for design of components. However, in the complex stress analysis for ductile materials, the von-Mises stress yield criterion is utilized [52]. The yield criterion of von-Mises stress is given as

$$\sigma_i = \sqrt{3J_2} = \sqrt{\frac{(\sigma_{11} - \sigma_{22})^2 + (\sigma_{22} - \sigma_{33})^2 + (\sigma_{33} - \sigma_{11})^2 + 6\left(\sigma_{11}^2 + \sigma_{22}^2 + \sigma_{33}^2\right)}{2}} \tag{2.14}$$

here J_2 represents second invariant of deviatoric stress, and σ_{11}, σ_{22}, ..., σ_{12}, σ_{13}, etc. are

components of the Cauchy stress tensor, as expressed below:

$$\sigma = \begin{bmatrix} \sigma_{11} & \sigma_{12} & \sigma_{13} \\ \sigma_{21} & \sigma_{22} & \sigma_{23} \\ \sigma_{31} & \sigma_{32} & \sigma_{33} \end{bmatrix} \qquad (2.15)$$

The von-Mises stress criterion is very commonly applied in automotive applications e.g. twin helical springs analysis [53] and stress estimation of automotive coil springs [54]. Several studies and conducted experiments have verified the accuracy level of the von-Mises stress evaluation method for the estimation of stress [55].

The failure of component is instantaneous in case of maximum stress in component exceeding the ultimate tensile strength of material. This category of failure is termed as static failure. Important aspects of component design comprise of selecting the material and determining the geometrical dimensions to ensure that component will sustain for lifetime needed for specific application and it will neither buckle nor deform beyond certain permissible limits. Nevertheless, it has been mentioned in literature article that static scenarios had never resulted in the failure of automotive coil springs [18, 56, 57]. The study express that repeated cyclic loading was significant factor in the failure of coil spring, as coil spring can sustain the static single load whereas vehicle in motion experiences iterative and continuous cyclic loading applied on the suspension system. Hence, durability analysis becomes important in fatigue life estimation of design to ensure coil spring is safe and operational throughout the desired lifespan of vehicle system.

2.4 Durability Analysis

Durability analysis is an important domain for automotive industries as fatigue failure can lead to severe losses. For ground vehicles, suspension components are very crucial for safe and smooth travel. Fatigue failure in suspension components, especially spring, could cause road accidents. The road accident can cause financial losses, vehicle damage and injuries to people riding in vehicle. Fatigue analysis of vehicle suspension component becomes mandatory in preventing potential losses, and encouraging safety of vehicle.

2.4.1 Durability Analysis and Design

Engineering researchers and automotive industries have acknowledged the importance of fatigue analysis. Several experiments in fatigue domain had been performed to improvise the design of vehicle components. A technique known as V-Cycle, was established to consider fatigue design of vehicle suspension components as shown below:
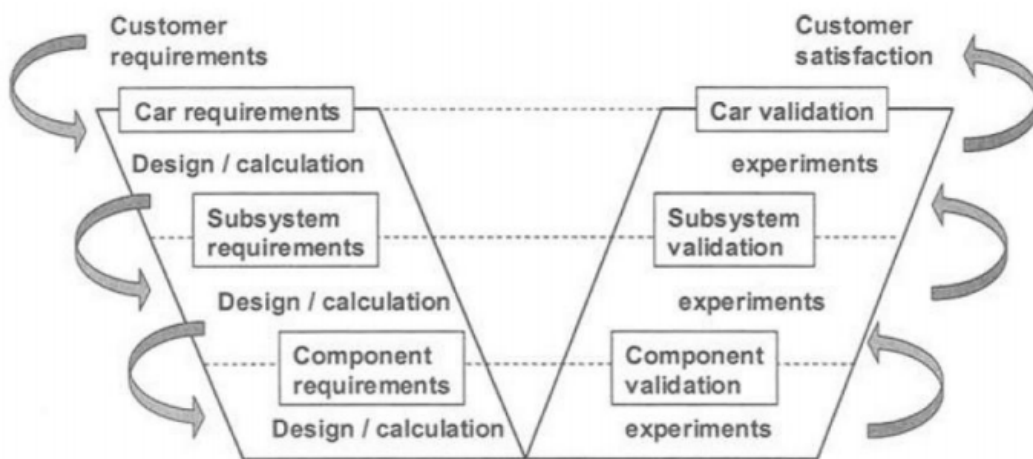
Figure 2.11: Fatigue Design Technique of Automotive Suspension System.
Source: Thomas et al [58]

The V-Cycle first consider the requirements of customer and later categorize the design requirements of vehicle into subsystems. Experimental results are used to validate the suspension component design. After gaining a good understanding of fatigue characteristics requirement, unnecessary material could be removed to reduce cost and achieve the optimisation of component design [59].

Durability analysis is performed for predicting the fatigue life of component. The process considers input as geometry, material property and service loadings. The procedures are collectively called the "Five - Box Trick" durability model, is described below:
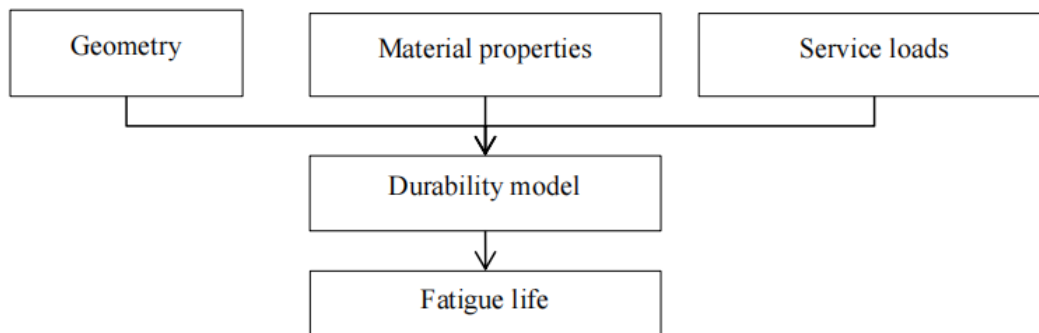
Figure 2.12: "Five - Box Trick" Durability Model.
Source: Karthik et al [60]

The geometry is utilized for determination of critical stress concentration region and distribution of fatigue life. In addition, assigning correct boundary conditions imitate the original experimental set up for fatigue analysis and generates relevant results. Material property, geometry and service loads are utilised together for the fatigue assessment which is clearly visualised in the Fig. 2.12 shown above.

In the past, numerous durability models have been implemented during the fatigue design process of automotive suspension. Various researches have used virtual simulation techniques for prediction of fatigue life in vehicle suspension components. The aim of analyses was reduction in weight of component and altogether sustaining the fatigue characteristics.

In addition, methodologies to model the road surface loadings for predicting fatigue life have drawn interest of researchers and automotive industry as well. Those studies focus on developing exact loading conditions generated from road surface profiles. The constructed road model is utilized for fatigue life assessment related to suspension components.

2.4.2 Classification of Road Surface Loading

Road surface can be expressed as a function having independent variables consisting details of loading induced from road profiles. Understanding the information carried by road surface, becomes crucial for durability and vehicle ride analyses. The exactness of road surface mapping to a function leads the precise durability analysis of automobile components. The road surface characteristics are first determined statistically for studying the dynamic behavior of an automobile. Fatigue property of vehicle component is influenced by behavior of road profiles [61]. Fatigue cyclic loadings are classified under two major types, having constant and variable amplitudes. Constant amplitude loading (CAL) can be expressed using a mathematical equation, e.g.

$$y = A \sin\left(\omega_0 t - \theta\right) \tag{2.16}$$

where A is loading amplitude, ω_0 and θ represent frequency and phase angle of loading respectively. The CAL consists of specific function over time and no variation is observed with time. The CAL can be represented in various forms as shown in Fig. 2.13. The CALs generate a complete pattern that gets repeated over time frame. For fatigue life assessment of automobile components, the manufactures utilize the CALs [60] as equivalent CALs being easy and convenient to execute for experimental testing of component in research labs.

27

Figure 2.13: CAL Representations: (a) Time Series, and (b) Peak-Valley Reversals.
Source: de Jesus and da Silva [62]

Variable amplitude loading (VAL) signifies random behavior of road profile load-
ing that cannot be expressed using mathematical equation as in case for CAL. The VALs
are broadly implemented in automobile industries. Multiple loading analysed for fatigue
assessment exhibit variable amplitude characteristics [63]. The VAL data was applied for
producing cyclic load in evaluation of vehicle fatigue life [64]. Another study implemented
VALs for analyzing the dynamic response of vehicle planetary gear [65]. Considering prac-
tical road operating scenarios, mostly loadings are expressed as VALS because road profiles
comprise of potholes or bumps [66].

For CAL cyclic loading scenarios, stress amplitude, σ_a, and mean stress, σ_m, can
be evaluated by mathematical expressions given as

$$\sigma_a = \frac{\Delta\sigma}{2} = \frac{\sigma_{max} - \sigma_{min}}{2} \tag{2.17}$$

$$\sigma_m = \frac{\sigma_{max} + \sigma_{min}}{2} \tag{2.18}$$

here $\Delta\sigma$ represents stress range, σ_{max} and σ_{min} are maximum and minimum stress values

28

respectively. For CAL fatigue assessment, the oscillating loading is implemented on automotive component along with mean stress, σ_m. Another parameter known as stress ratio, R, as defined in Eq. 2.19 , is utilized for representing the mean stress during fatigue testing of component. Multiple stress ratios were used for evaluating the fatigue behavior of high strength steel during generation of S-N curve [67].

$$R = \frac{\sigma_{min}}{\sigma_{max}} \tag{2.19}$$

In CAL scenarios, determination of stress ratio and analysing various parameters are convenient for fatigue assessment. The behavior of multiple parameters were observed on nitride steels during growth of fatigue cracks under CAL conditions [68]. It was also mentioned than VAL was not important for their analysis as loading applied consisted of an independent variable. Fatigue assessment of component under VAL and CAL are completed distinct. Most of loading applications in real world comprise of stress amplitudes exhibiting irregular characteristics.

The VAL comprises of no definite pattern as shown in Fig. 2.14, and the cyclic loading oscillates in between varying minimum and maximum value of amplitudes. A study was performed for analysing the behavior of fatigue life under CAL and VAL scenarios [69]. The experiment outcome expressed that fatigue evaluation of component was lower in VAL than measured under CAL for equivalent range of stress. Another experiment was conducted using VAL for determination of crack growth under fatigue for various combination of overload (OL) and underload (UL) conditions. It was observed that for OL scenario, the overall crack fatigue life got increased also called a crack retardation, and the fatigue life decreased (known as crack acceleration) under UL application [70]. The implementation of VAL for study of crack initiation, and growth under fatigue are quite distinct.
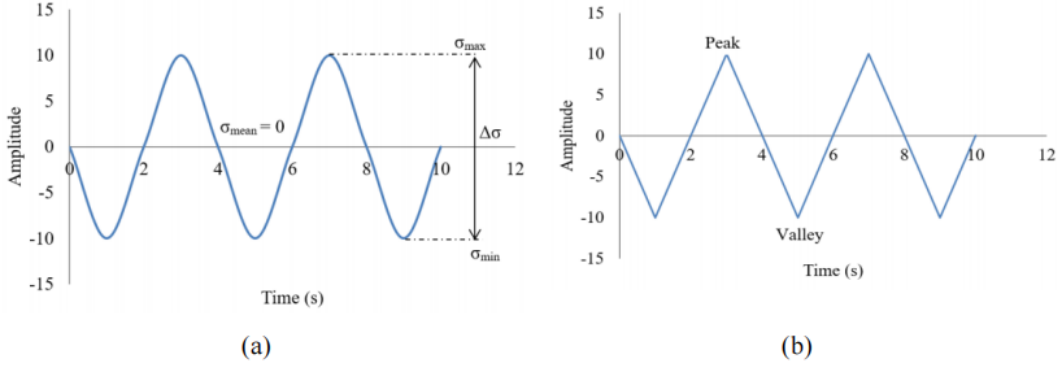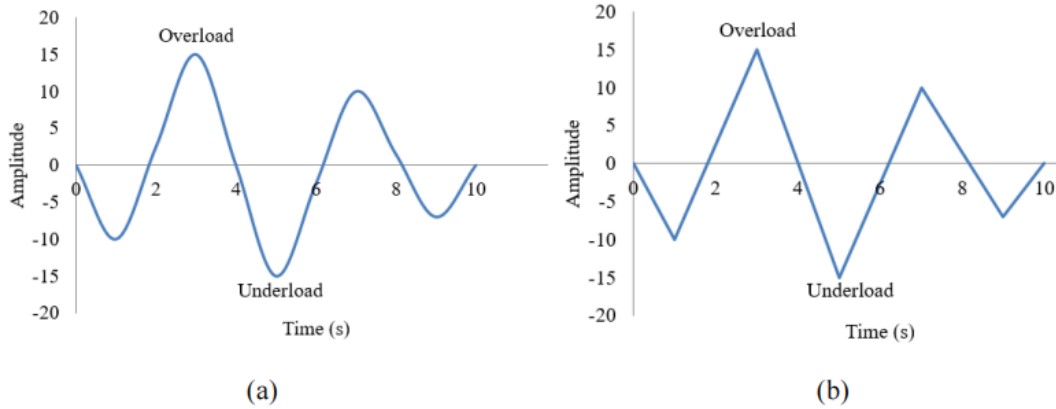
Figure 2.14: VAL Representations: (a) Time Series, and (b) Peak-Valley Reversals.
Source: de Jesus and da Silva [62]

For engineering applications, VALs are included as a component of entire design process. Considering efficient and robust analysis, actual VAL are transformed to an equivalent damage load as assessment of VAL are excessive time taking and costly process [58]. The VAL had been broadly applied in automobile industry for study of fatigue behavior in vehicle suspension components [71, 72, 73]. Load time histories are utilized in automobile industry in various forms e.g. stress, strain or force. Few studies had concentrated on transforming VAL to CAL for fatigue assessment of vehicle components. This signifies the importance of mapping road surface loading for durability analysis of automotive suspension.

2.4.3 Fatigue Life Analysis

Fatigue life of specimen is described by counting the stress cycles prior to failure occurrence of a particular nature. There are two classification of fatigue life evaluation techniques, low and high cycle fatigue (LCF and HCF). The LCF is considered below 1×10^4 cycles while HCF occurs above 1×10^4 cycles. Considering LCF, total fatigue life of specimen consists of crack characteristics e.g. initiation and propagation of crack. Very high cycle fatigue (VHCF) is expressed as occurrence of fatigue life above 1×10^7 cycles [74]. Mechanical

rotating components e.g. turbine blades are designed considering HCF as the components are exposed to multiple cyclic loadings or large frequency vibrations [75].

Regular periodic maintenance of component or structure is needed for preventing the fatigue failure [76], and prognostics health monitoring can be used for scheduled maintenance [77, 78]. The fatigue preventive techniques are feasible economically for large and expensive products e.g. aircraft, as the replacement cost is extremely high, whereas for small mechanical components such as vehicle steering, automotive engine and suspension component, those methods are not suitable. Replacement of small mass-produced components, after the service period, is simple feasible approach for prevention of fatigue failure [79]. With the initiation of crack in component, it is determined as failed. A study was conducted for evaluating effect of crack length on fatigue life of spring steel [80]. It was mentioned that crack length under 0.2 mm can be considered as safe for spring material.

Crack is initialised due to concentration of stress at a critical location and stress life (S-N) technique was utilised for assessing the fatigue characteristics of component. The S-N approach was proposed by A. Wöhler for determination of fatigue feature which could further lead to actuation of cracks. The S-N method is still broadly used by researchers [81]. The mean stress and amplitude stress are two important parameters for fatigue assessment using S-N approach. For an initial model in 1874, inclusion of mean stress effect was suggested by W. Gerber. Tension and compression effects were not considered in proposed model. The model was updated to more conservative form by J. Goodman in 1914. Again in 1930, C. R. Soderberg reformulated existing Goodman model considering the yield strength. Soderberg model being conservative and expecting no occurrence of fatigue failure nor yield [82]. For the Gerber, Goodman and Soderberg models, only tensile loading scenarios are considered.

The two *S-N* curve constants, σ'_f and b, for four different types of steels, considering zero mean stress, are tabulated below [7]:

Table 2.3: *S-N* Curve Constants at Zero Mean Stress, $\sigma_m = 0$.

Types of Steel	σ'_f (MPa)	b
SAE 1015	1020	-0.1380
SAE 4142	1937	-0.0762
AISI 4340	1758	-0.0977
SAE 5160	2063	-0.0800

here σ'_f represents fatigue strength coefficient, and b represents fatigue strength exponent for steel materials. During this research, SAE 5160 carbon steel is material selected for suspension spring. Referring to data from Table 2.3 and using the Eq. 2.20, the *S-N* curve for different types of steel are plotted below:
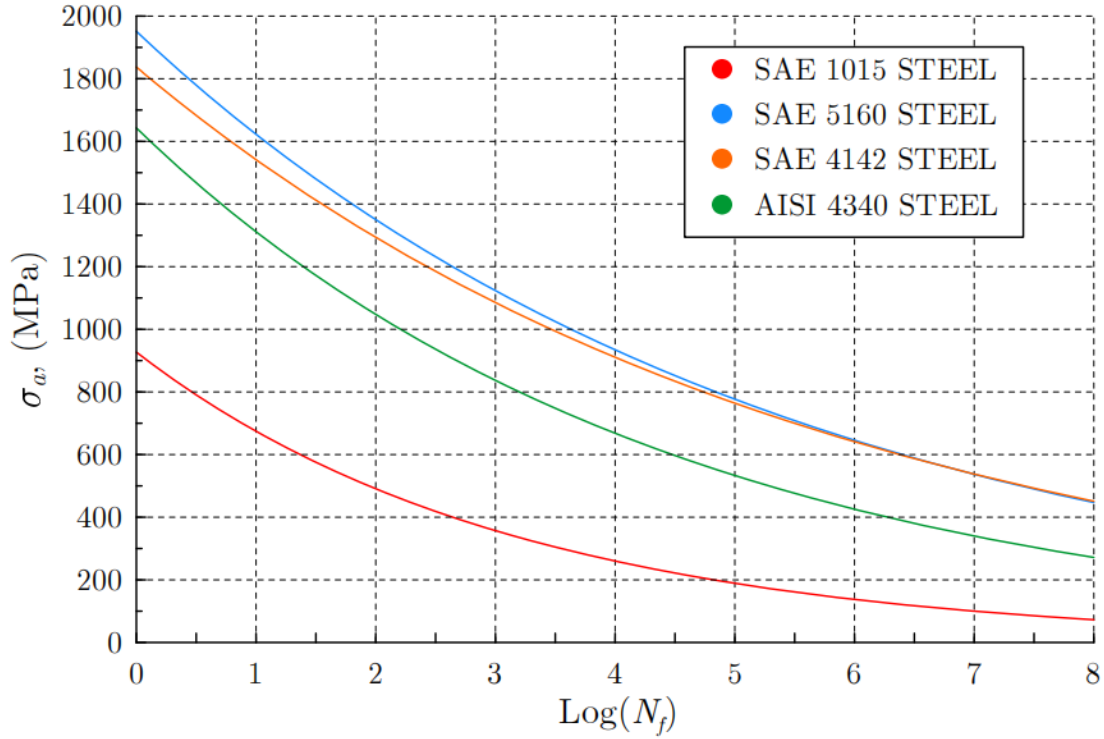
Figure 2.15: *S-N* Curve for Various Steels.

Considering the correction in mean stress, fatigue life of component can be predicted using a mathematical relation. The fatigue life prediction model is mathematically expressed as mentioned below:

$$\sigma_a = \sigma_f' \left(2N_f\right)^b \tag{2.20}$$

For nonzero value of mean stress, σ_m, the above equation yields to a general stress-life relation described as [7]

$$\sigma_a = \left(\sigma_f' - \sigma_m\right) \left(2N_f\right)^b \tag{2.21}$$

here σ_a is induced stress, σ_f' represents coefficient of fatigue strength, N_f is cycles count prior to fatigue, and b represents exponent of fatigue strength. The Goodman model is considered conservative where load scenarios are dominant with tensile behavior [60], while the Gerber model is selected in case of zero-mean loading. The *S-N* technique is appropriate for structure or component requiring high factor of safety. The *S-N* approach is utilized where better accuracy exists for component having only higher fatigue life, in the range of 10^5 cycles [83]. There is another method for fatigue life assessment, which is strain life approach (ϵ-*N*), that considers material behavior under varying load with time, such as cyclic hardening effects.

The ϵ-*N* method provides better accuracy in fatigue life assessment of component [84]. This technique considers plastic deformation in nearby region of fatigue crack origin [85]. The ϵ-*N* curve behavior of steel material is described by Fig. 2.16. The curve marked with "Total" label expresses the ϵ-*N* model, and it is obtained using both elastic and plastic data sets. ϵ-*N* approach is implemented for component made up of ductile material having low cycle fatigue in range of 10^3 life cycles. Both the techniques, *S-N* and ϵ-*N*, are
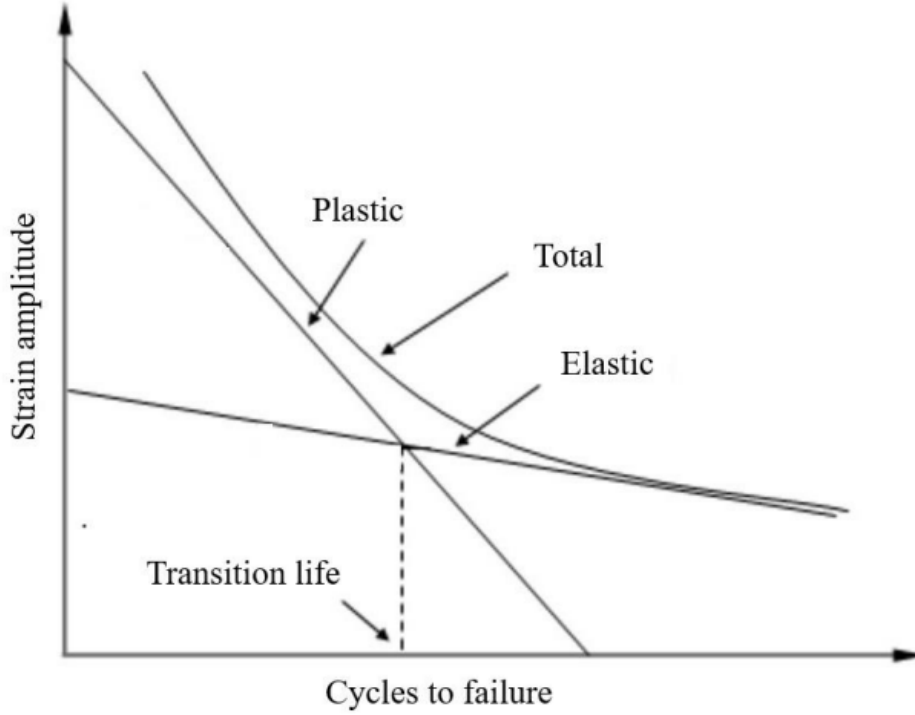
Figure 2.16: Typical ϵ-N Curve for Steel.
Source: Williams et al [86]

not applicable for growth and propagation of cracks. It is mentioned that elastic linear be-

havior of ϵ-N model is obtained from a relationship provided by O.H. Basquin in 1910 [87].

S.S. Manson proposed a mathematical relation for plastic strain in 1954 which is

$$\epsilon_p = \epsilon'_f \left(2N_f\right)^c \tag{2.22}$$

here ϵ_p is plastic strain, ϵ'_f and c represents coefficient of fatigue ductility and exponent of

fatigue ductility respectively. Later, Coffin-Manson relationship was obtained considering

both elastic and plastic strains. This relationship is the first ϵ-N mathematical model that

correlates fatigue life and strain, as mentioned below:

$$\epsilon_p = \frac{\sigma'_f}{E} \left(2N_f\right)^b + \epsilon'_f \left(2N_f\right)^c \tag{2.23}$$

Consideration of mean stress effect is significant for fatigue life evaluation with both S-N and ϵ-N methods, as mean stress is a segment of fatigue failure criterion [7, 83]. The Coffin-Manson relationship provided acceptable outputs when compared with different fatigue models [88]. However, it was observed that this relationship could not fit the data well for small plastic strain [89]. Also, this relationship exhibits the limitation with components subjected to multiple mean stresses. In real world applications, tensile (positive) and compressive (negative) mean stresses tend to reduce and increase the fatigue life of components respectively [90, 91, 92, 93]. Hence, few automobile components e.g. gears, are induced with compressive stress for enhancing their fatigue lives [94]. In 1968, J.D. Morrow proposed strain-life model to adjust the mean stress effect in the ϵ-N curve. In Morrow strain-life model, the mean stress, σ_m, was included to Coffin-Manson relationship which can be mathematically expressed as

$$\epsilon = \frac{\sigma_f^{'} - \sigma_m}{E} \left(2N_f\right)^b + \epsilon_f^{'} \left(2N_f\right)^c \tag{2.24}$$

The value of σ_m is positive for tensile loading, and negative for compressive loading. Considering the fatigue assessment of spot weld joint, Coffin-Manson model provided better results as compared to Morrow strain-life relationship [95].

Another ϵ-N model was proposed by K.N. Smith, P. Watson and T.H. Topper in 1970. This Smith-Watson-Topper (SWT) model is broadly applied for fatigue assessment [85]. The mathematical representation of SWT model is expressed using Eq. 2.25.

$$\sigma_{max}\epsilon = \frac{\left(\sigma_f^{'}\right)^2}{E} \left(2N_f\right)^{2b} + \sigma_f^{'}\epsilon_f^{'} \left(2N_f\right)^{b+c} \tag{2.25}$$

The two model parameters, maximum stress, σ_{max}, and strain amplitude per cycle, were evaluated from fatigue testing results, and obtained using multiple mean stress and various

stress or strain amplitude values. The SWT relationship is robust and acceptable for broad range of materials [85], while fatigue life evaluation obtained from Morrow approach holds good only for steel [96].

There is a technique opted for fatigue life assessment through computation of a damage parameter on cycle basis. The SWT model provided acceptable results under tensile load conditions, while Morrow approach predicted better fatigue life for compressive loading on automotive component made of steel material [97]. It was stated that the SWT model is more flexible, and holds good for fatigue life assessment for several practical applications [85]. Both Morrow and SWT approaches are utilized for fatigue evaluation under zero mean stress as well [60]. Considering zero mean stress, Morrow model and Coffin-Manson relationship are equivalent. Each model provides specific interest or mean amplitude value of strain for fatigue damage estimation. Finally, accumulated total damage under fatigue is utilized for complete fatigue life assessment.

2.5   Current Research

The dynamic analysis was conducted on helical coil spring, and performance of multiple finite elements were compared to provide an easy and reliable approach in area of spring design [98]. Jugulkar et al analysed the suspension system for varying stiffness and damping forces used for automotive application [99]. The quarter car model was applied in this study for quantifying ride comfort and assessment of vehicle handling. Dong conducted a recent study in 2020, which compared the performance of ordinary vehicle suspension coil spring with variable-parameter coil compression spring, based on load-deformation behavior and stress distribution characteristics [100]. Another study was performed by Yildirim and

36

Ince on helical springs having different shapes to investigate the natural frequencies, behavior under axial and shear deformations, and effects of rotary inertia [101]. Becker et al conducted a research that produced frequency design charts for coil spring having circular cross-section and clamped ends, under static axial compression loading [102]. The linear equations that governed resonance frequencies of helical spring were solved using transfer matrix approach, and investigation of effect of variation in number of coil turns was conducted. Also, this research validated previous work done by modelling the helical spring as an elastic beam with rigidities for bending, compression and shearing.

The study conducted in 2011, provided description and review of various automotive suspensions, and the authors compare suspensions considering multiple parameters e.g. ride comfort, weight, dynamic performance, structure, energy recovery etc [103]. Lavanya et al investigated safe loading on automotive suspension helical spring using different materials [54]. This research was performed in 2014, and it compared overall stress and deformation of spring for selected materials, and proposed the acceptability for optimum design and analysis. Another research focused on weight reduction of automobile coil spring by replacing steel with composite materials [104]. This study utilized numerical and experimental methods for attaining spring rate equivalent to a steel spring component. The outcome from finite element model of optimized composite spring was compared with experimental results.

Sun et al conducted a research on high speed vehicles, and utilized dynamic stiffness matrix approach to evaluate dynamic stiffness of helical coil spring used in vehicle suspension [105]. Under this research, FEA was conducted to compare the results, and the behavior of spring dynamic stiffness on vehicle vibration was studied. In 2019, a study performed by Pastorcic et al described the failure and fatigue analyses conducted on helical spring of automotive passenger vehicle [106]. In this research, various experimental techniques were applied for fracture assessment, and finite element model of helical spring was analyzed for

dynamic loading scenarios. Also, quarter car model was implemented to evaluate the vehicle behavior, and results obtained from the analysis were useful in predicting the spring fatigue characteristics and futuristic design optimization of automotive spring. Putra et al studied the failure analysis of automotive suspension spring, and stated that inner surface was harder as compared surface of coil spring and maximum stress concentration at a point in spring resulted in the initiation of early cracks [107]. Another recent study performed in 2020, proposed a dynamic model to understand and analyse the various influential factors contributing to induced abnormal vibrations, which further led to failure of vehicle suspension coil spring [108].

Multiple studies had been conducted in 2017 and 2018, focused on analysing the loading profiles generated by the unevenness of various road surfaces which significantly influence the fatigue characteristics of suspension coil spring [109, 110, 111]. Strain signals were acquired for analysis from suspension spring, and these studies aimed at generating more accurate road loading profiles, and predicting realistic fatigue life behaviour of suspension spring. Another research was conducted for determining fatigue life of automotive suspension coil spring considering different vehicle speeds [112, 113]. The ϵ-N approach was utilised for fatigue assessment of coil spring, and this research highlighted that roughness of road surface along with driving behavior e.g. turns, acceleration, braking etc significantly affected the component life of vehicle. In 2018, Kong et al conducted a study to evaluate vibrational fatigue analysis of automotive coil spring, using frequency-based approach under different road excitation scenarios [114]. In this analysis, acceleration signals from suspension were converted to PSD, and different cycle counters obtained equivalent load cycles. The S-N method was utilised for assessing the fatigue life of coil spring, using the stress response obtained using a spring FRF, equivalent load cycles, and various stress criterion.

Kong et al discussed the MLR model for predicting the fatigue life of vehicle spring [115]. The MLR model was developed considering the Coffin-Manson, Morrow, and Smith-Watson-Topper strain-life models. The durability model utilised weighted vehicle acceleration (vibrations), and natural frequencies as inputs for fatigue assessment. The results predicted by various models were validated and compared with prediction from strain measurements. The same authors conducted another study, using HMLP ANN model for fatigue evaluation of suspension coil spring [116]. The study implemented quarter car model for conducting the simulations using acceleration signals and artificial road surface profile as inputs. After validating results, researchers mentioned that optimised HMLP ANN model performed the fatigue life assessment of automotive suspension spring with acceptable range of accuracy.

Chin et al performed two studies for durability assessment of vehicle suspension coil spring, first study considered multifractal analysis of road excitations [117], and the second study focused on strain generation using simulation of MBD [118]. The models established in both the studies generated durability assessment of coil spring under allowable range of accuracy, thus reducing the requirement of real measurement of strain data at suspension coil spring. The cohesive zone modeling is popularly used for modeling fatigue crack initiation and propagation [119]. In the recent work by Karthik et al, a framework has been developed for probabilistic fatigue life prediction by integrating cohesive zone modeling, machine learning and statistical techniques [120, 121].

Chapter 3

DYNAMICS OF SPRING

3.1 Introduction

Passenger vehicles require the suspension system to have simple operation mechanism, and utilize less space in the vehicle. Macpherson suspension system suited well, and fulfilled the requirement as compared to double wishbone type of suspension system. Although, both the suspension systems, Macpherson and double wishbone types, have good endurance strength and good durability. In this study, helical coil spring of front suspension system was utilized for performing the stress and fatigue life analysis. The methodologies opted to perform the analysis has been described in the subsequent sections.

3.2 Mechanics of Coil Spring

3.2.1 Static Load-Deformation Relation

Multiple researches and experimental work have been conducted to study the properties of helical springs. Thomson and Tait [122] and Love [123] performed analyses to derive geometrical relationship between spring parameters, e.g. static load, pitch angle and curvature of coil. The work of Love [123] describes the static response of helical spring by deriving

equilibrium equations. A helical spring is commonly considered as linear compression and extension element, in which deformation is proportional to applied force. In fact, Jiang et al [124] mentioned that spring is a non-linear mechanical component, where torsional deformation consistently accompanies compressive and extensional deformation of spring, and vice versa.

Figure 3.1 describes static displacement of spring, $\delta_{initial}$, under application of axial compressive preload, F, due to quarter weight of vehicle.
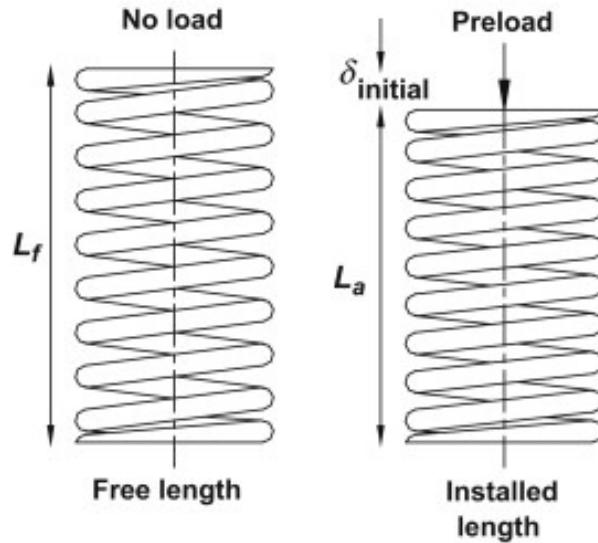
Figure 3.1: Static Displacement, $\delta_{initial}$, under Preload Condition.
Source: Childs [45]

Considering the design theory of helical compression spring, an axially loaded spring behaves like a straight bar element under pure torsion, and the shear stress, τ, across the cross-section of spring wire is expressed as [125]

$$\tau = \frac{8FD}{\pi d^3} \tag{3.1}$$

here D and d represent mean coil diameter, and spring wire diameter. Also, the total static

deflection of spring, $\delta_{initial}$, caused from the total angular torsion, ϕ, is given as [125]

$$\phi = \int_0^{\pi D N_a} \frac{2\tau}{Gd} \, dx = \int_0^{\pi D N_a} \frac{16FD}{\pi G d^4} \, dx = \frac{16 F N_a D^2}{Gd^4} \tag{3.2}$$

$$\delta_{initial} = \frac{D\phi}{2} = \frac{8 F N_a D^3}{Gd^4} \tag{3.3}$$

here G represents modulus of rigidity, and N_a is number of active coils. The expression for spring stiffness, K, is evaluated using Hooke's law (Eq. 2.2) is described below [125]:

$$K = \frac{F}{\delta_{initial}} = \frac{Gd^4}{8 N_a D^3} \tag{3.4}$$

3.2.2 Governing Equations of Spring Motion

Johnson [126], Dick [127], Geballe [128], Wittrick [129], Kagawa [130], Phillips and Costello [131], Stokes [132], Costello [133], and Sinha and Costello [134] discussed the dynamic response of helical spring. Michell [135] derived three governing differential equations of motion to describe spring dynamics, using Lagrange's equation. Love [136] expressed six spring motion equations, considering the Michell's assumptions. Lin and Pisano [137] derived the dynamic equations describing the spring motion, having varying helix radius and pitch angle, using Hamilton's principle is mentioned below:

$$\int_{t_1}^{t_2} \delta \left(\sum T_i - \sum U_i \right) dt = 0 \tag{3.5}$$

where $\sum T_i$ and $\sum U_i$ are total kinetic and total potential energies from elastic strain in helical spring respectively. Four equations of motion were formulated by applying the Hamilton's

principle and variational methods. In this research, the dynamic equations were reduced to simplified forms and comparison was performed with pre-existing spring equations of motion.

Jiang et al [138] investigated the extensional and torsional dynamic characteristics of helical spring, and expressed the linear force-strain relationships, that are

$$F = k_1\epsilon + k_2\phi$$
$$M = k_3\epsilon + k_4\phi$$

(3.6)

here F is axial force, M is twisting moment, ϵ is axial strain, ϕ is rotational strain, and

$$
\begin{aligned}
k_1 &= \frac{\pi E R^4}{r^2 \Delta}\left[1 + k^2\left(1+\nu\right)\right] \\
k_2 &= -\frac{\pi \nu E R^4 k}{r\Delta} \\
k_3 &= -\frac{\pi E R^4 k}{4r\Delta}\left(4\nu + \frac{R^2}{r^2}\right) \\
k_4 &= \frac{\pi E R^4}{4\Delta}\left[4\left(1+\nu+k^2\right) + \frac{k^2 R^2}{r^2}\right]
\end{aligned}
$$

(3.7)

are stiffness constants. In Eq. 3.7, R is spring wire radius, r is radius of helix, k is tangent of helix angle α, and

$$\Delta = \frac{1}{k\sqrt{1+k^2}}\left[4\left(1+\nu\right)\left(1+k^2\right)^2 + \frac{k^2 R^2}{r^2}\left[\left(1-\nu\right) + k^2\left(1+\nu\right)\right]\right]$$

(3.8)

Considering the linear force-strain relationships, Eq. 3.6, the equations of spring motion for small deformations are [138]

$$k_1\frac{\partial^2 u}{\partial x^2} + k_2\frac{\partial^2 \theta}{\partial x^2} = \gamma\frac{\partial^2 u}{\partial t^2}$$

(3.9)

43

$$k_3\frac{\partial^2 u}{\partial x^2} + k_4\frac{\partial^2 \theta}{\partial x^2} = \mu\frac{\partial^2 \theta}{\partial t^2} \tag{3.10}$$

where $u(x,t)$ and $\theta(x,t)$ are axial and rotational displacements at specific time t, γ is mass and μ is mass moment of inertia about axis per unit length of spring in undeformed configuration respectively.

3.2.3 Dynamic Analysis of Vehicle System

The method based on degree of freedom (DOF) is utilised to analyse the vibrations induced in vehicle. The mass-spring-damper system as described in Fig. 3.2 having single DOF was considered in this study, based on an assumption that vibrations are transmitted in each
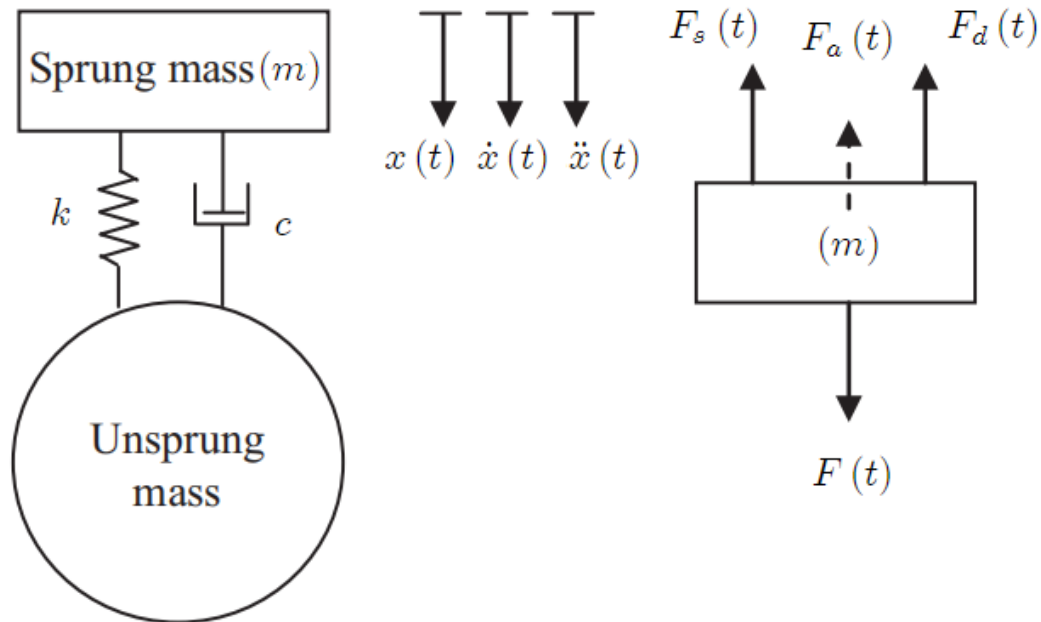
Figure 3.2: Free Body Diagram of Single DOF Mass-Spring-Damper System.
Source: Putra et al [110]

suspension independently without affecting other suspensions. The motion of mass-spring-damper system is initiated by applied force, $F(t)$. The governing equation of motion of

44

system, as obtained from Newton's second law, is

$$F_a\left(t\right) = F\left(t\right) - F_s\left(t\right) - F_d\left(t\right) \tag{3.11}$$

where spring force $F_s(t)$, damping force $F_d(t)$, and inertia force $F_a(t)$ are expressed in terms of dynamic quantities of the system, as mentioned below:

$$
\begin{aligned}
F_s\left(t\right) &= kx(t) \\
F_d\left(t\right) &= c\dot{x}(t) \\
F_a\left(t\right) &= m\ddot{x}(t)
\end{aligned}
\tag{3.12}
$$

Equation of motion after substituting the above expressions, is second-order linear ordinary differential equation with constant coefficients having m, c and k representing system parameters, takes the form

$$m\ddot{x}(t) + c\dot{x}(t) + kx(t) = F\left(t\right) \tag{3.13}$$

For a damped forced vibration, the equation of motion for mass-spring-damper system is represented by Eq. 3.13. The left side of equation specifies internal forces, and right side represents external forces. Vibrations are transferred to the vehicle suspension spring through wheels while travelling on uneven road terrain. The quarter vehicle model comprising of sprung mass, m, spring stiffness, k, and damper coefficient, c, is considered for analysis. The road surface model utilised in this research is described as shown in Fig. 3.3. The vehicle model is traveling with horizontal velocity, V, over the sinusoidal road surface model having wavelength, L.
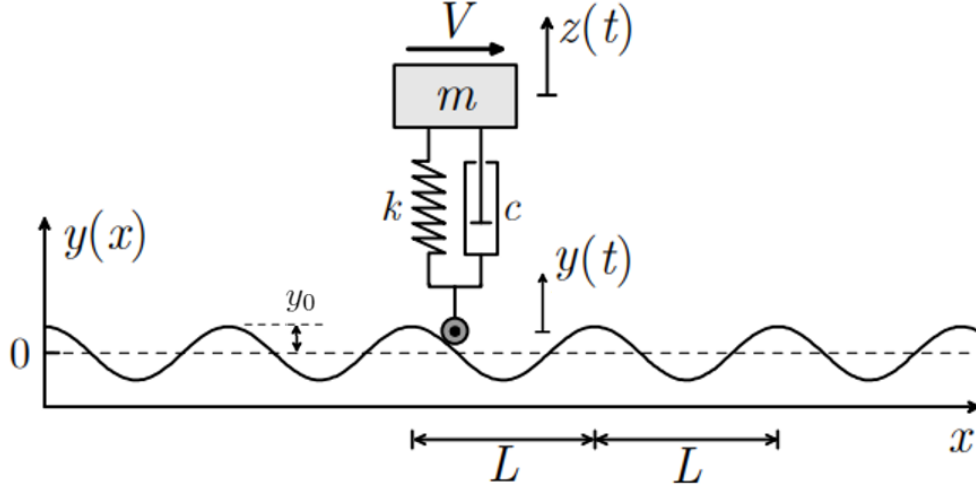
Figure 3.3: Quarter Vehicle Model Traveling on Wavy Road Surface.
Source: Thangjitham [139]

The harmonic excitation in wheel passing over road surface is represented as

$$y(t) = y_0 e^{i\omega t} \tag{3.14}$$

here y_0 and ω are magnitude and frequency of excitation, respectively. Considering the Newton's second law, the governing equation of motion of sprung mass (m) is

$$m\ddot{z}(t) + c\dot{z}(t) + kz(t) = c\dot{y}(t) + ky(t) \tag{3.15}$$

or

$$\ddot{z}(t) + 2\zeta\omega_n\dot{z}(t) + \omega_n^2 z(t) = 2\zeta\omega_n\dot{y}(t) + \omega_n^2 y(t) \tag{3.16}$$

here ω_n is natural angular frequency of system, and ζ is damping factor, that are defined as

$$\omega_n = \sqrt{\frac{k}{m}} \tag{3.17}$$

46

$$\zeta = \frac{c}{2\sqrt{km}} \tag{3.18}$$

The mathematical expressions to evaluate response of sprung mass, m, and force transmitted to spring traveling on road surface model (Fig. 3.3) are discussed in subsequent sections.

3.2.3.1 Transmissibility of System

After substituting the characteristics of wheel excitation into governing equation of motion (Eq. 3.16), the response of mass m is obtained as $z(t)$, as expressed below:

$$z(t) = y_0 G(\omega) e^{i\omega t} = y_0 |G(\omega)| e^{i(\omega t - \phi)} \tag{3.19}$$

here $G(\omega)$ is the frequency response, $|G(\omega)|$ is known as transmissibility, and ϕ is the phase angle, which are defined as

$$G(\omega) = \frac{1 - \left(\frac{\omega}{\omega_n}\right)^2 + \left(2\zeta\frac{\omega}{\omega_n}\right)^2}{\left(1 - \left(\frac{\omega}{\omega_n}\right)^2\right)^2 + \left(2\zeta\frac{\omega}{\omega_n}\right)^2} - i\frac{2\zeta\left(\frac{\omega}{\omega_n}\right)^3}{\left(1 - \left(\frac{\omega}{\omega_n}\right)^2\right)^2 + \left(2\zeta\frac{\omega}{\omega_n}\right)^2} \tag{3.20}$$

$$|G(\omega)| = \frac{\sqrt{1 + \left(2\zeta\frac{\omega}{\omega_n}\right)^2}}{\sqrt{\left(1 - \left(\frac{\omega}{\omega_n}\right)^2\right)^2 + \left(2\zeta\frac{\omega}{\omega_n}\right)^2}} \tag{3.21}$$

$$\phi(\omega) = \tan^{-1}\frac{2\zeta\left(\frac{\omega}{\omega_n}\right)^3}{1 - \left(\frac{\omega}{\omega_n}\right)^2 + \left(2\zeta\frac{\omega}{\omega_n}\right)^2} = \tan^{-1}\frac{2\zeta\left(\frac{\omega}{\omega_n}\right)^3}{1 - (1 - 4\zeta^2)\left(\frac{\omega}{\omega_n}\right)^2} \tag{3.22}$$

The plot of transmissibility, $|G(\omega)|$, and frequency ratio, ω/ω_n for different values of ζ is shown below:
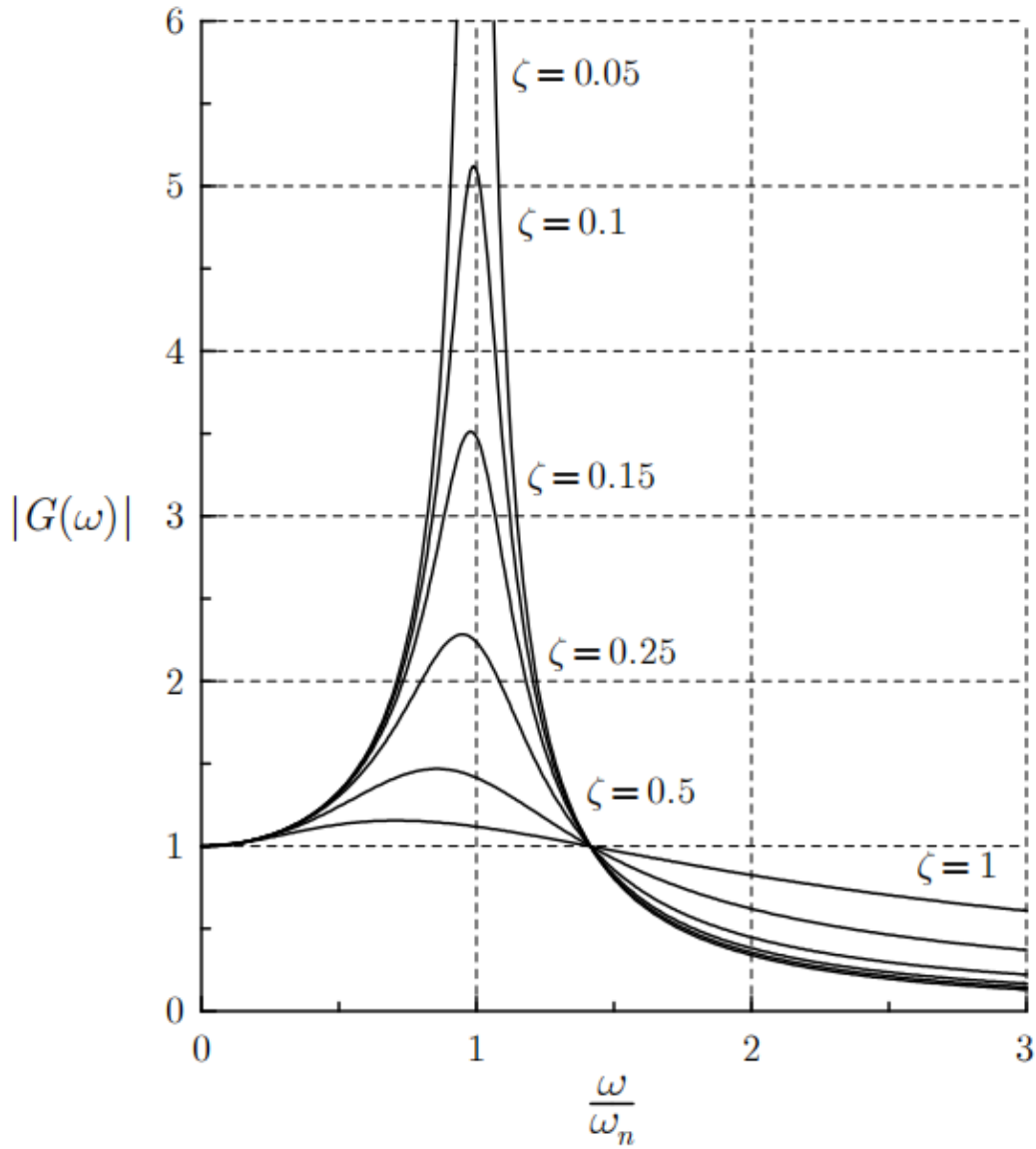
Figure 3.4: Transmissibility Curve for Different Frequency Ratios.

The resonance behavior is clearly visualised in the form of vertical peaks near the value of frequency ratio, ω/ω_n, close to unity. As the value of damping factor, ζ, becomes zero, the peak value of transmissibility of vehicle system approaches to infinity. Also, with increase in

damping factor value from zero to unity, there is shift in the vertical peak towards the left direction. For larger values of frequency ratio, ω/ω_n, the slope of curve move towards zero i.e. curve becomes horizontal, and magnitude of transmissibility approaches to zero.

3.2.3.2 Force Response of Helical Suspension Spring

The excitation force transmitted to the spring, is evaluated considering net displacement and using the free body diagram, is expressed as

$$F_s(t) = k\left[y(t) - z(t)\right] = ky_0 G_1(\omega)e^{i\omega t} = ky_0|G_1(\omega)|e^{i(\omega t - \psi)} \tag{3.23}$$

where $|G_1(\omega)|$ is the magnification factor of force response. The parameters $G_1(\omega)$, $|G_1(\omega)|$, and ψ are defined below:

$$G_1(\omega) = \frac{\left(\frac{\omega}{\omega_n}\right)^2\left[\left(\frac{\omega}{\omega_n}\right)^2 - 1\right]}{\left(1 - \left(\frac{\omega}{\omega_n}\right)^2\right)^2 + \left(2\zeta\frac{\omega}{\omega_n}\right)^2} - i\frac{2\zeta\left(\frac{\omega}{\omega_n}\right)^3}{\left(1 - \left(\frac{\omega}{\omega_n}\right)^2\right)^2 + \left(2\zeta\frac{\omega}{\omega_n}\right)^2} \tag{3.24}$$

$$|G_1(\omega)| = \frac{\left(\frac{\omega}{\omega_n}\right)^2}{\sqrt{\left(1 - \left(\frac{\omega}{\omega_n}\right)^2\right)^2 + \left(2\zeta\frac{\omega}{\omega_n}\right)^2}} \tag{3.25}$$

$$\psi(\omega) = \tan^{-1}\frac{2\zeta\left(\frac{\omega}{\omega_n}\right)}{\left(\frac{\omega}{\omega_n}\right)^2 - 1} \tag{3.26}$$

The plot of magnification factor of force response, $|G_1(\omega)|$, and frequency ratio, ω/ω_n for

different values of ζ is shown below:
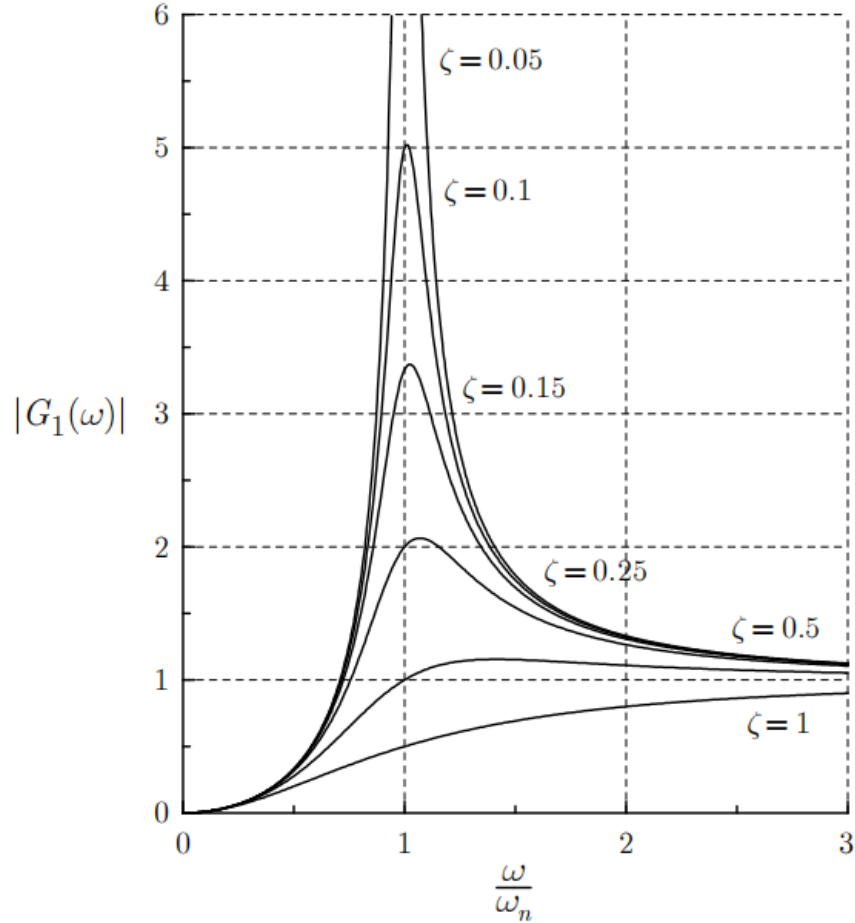
Figure 3.5: Plot of Force Response Magnification Factor and Frequency Ratio.

The vertical peak signifies the resonance condition, which is clearly visualised near the value of frequency ratio, ω/ω_n, close to one. For a particular value of frequency ratio, with the increase in value of damping factor, ζ, the force response magnification factor decreases. As the value of ζ becomes zero, the peak value of force response of suspension spring approaches to infinity. Also, with increase in damping factor value from zero to one, there is shift in the vertical peak towards the right direction. For larger values of frequency ratio, ω/ω_n, the slope of curve move towards zero i.e. curve becomes horizontal, and magnitude of force response magnification factor approaches to unity.

3.3 Finite Element Analysis on Coil Spring

The 3D geometry model of the helical spring is used as input for performing static, modal, and harmonic analyses. This section discusses meshing element, applied boundary conditions, and the formulation of finite element method. The mathematical equations to be solved during static and frequency response analyses have been expressed in the subsequent sections.

3.3.1 Geometry and Material Properties of Spring

The dimensions of suspension spring is comparable to 5-seater 1300 cc sedan passenger vehicle having 1085 kg of curb weight. The geometry of automobile suspension spring, used for the analysis, has been tabulated below:

Table 3.1: Geometrical Parameters of Helical Compression Spring.

Spring free length, L_f	360 mm
Mean coil diameter, D	120 mm
Spring wire diameter, d	12 mm
Total coils count, N	8
Number of active coils, N_a	6
End condition	Squared and Ground
Orientation	Counter-clockwise
Direction of wind	Left-handed

The spring model has been generated using the 3D computer aided design (CAD) program, SolidWorks®. The geometrical model of coil spring shown in Fig. 3.6 (a) and (b) consists of total eight coils, and describes the connection between spring and vehicle as shown in Fig. 2.1 and Fig. 2.2. The weight of suspension spring model, considering only eight coils, comes out to be 2.65 kg. The 3D CAD model of helical spring having six active coils, as described in Fig. 3.6 (c), is the finite element model which is utilised for static and dynamic FEA using Ansys Workbench™ software package.
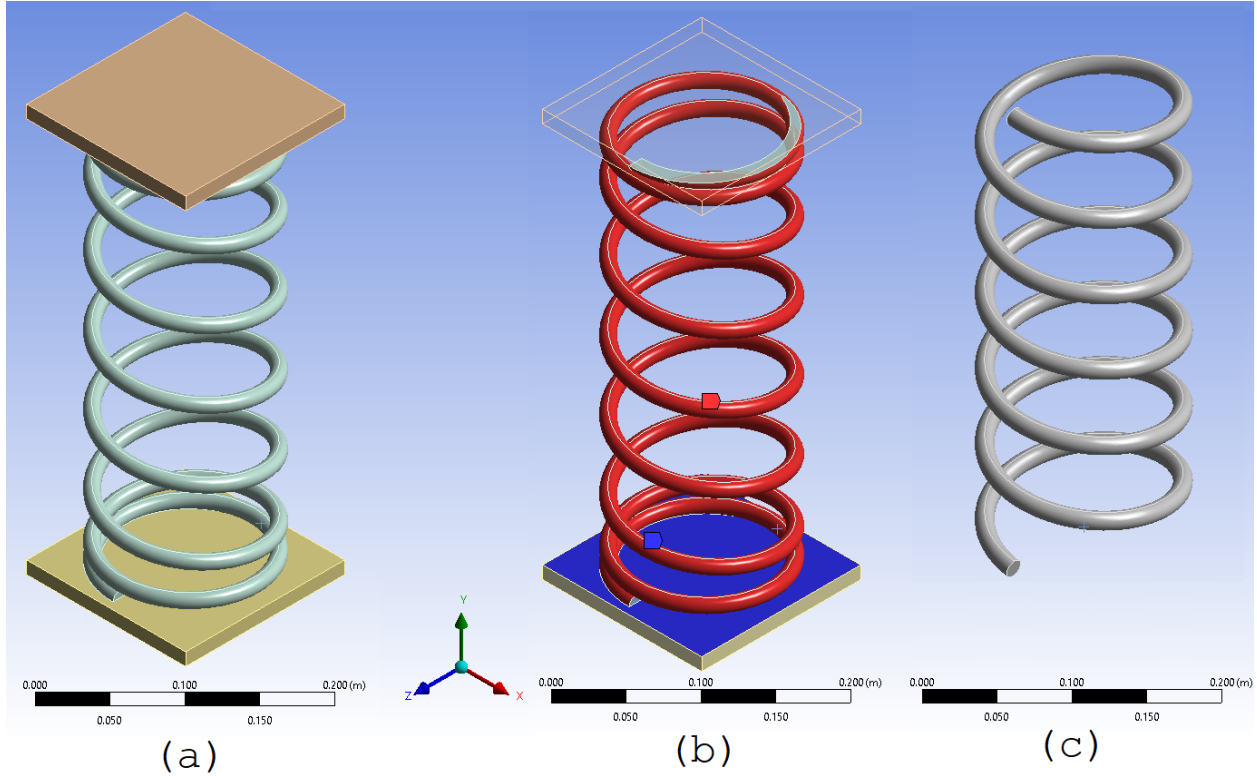
Figure 3.6: CAD Model of Helical Coil Spring.

Virtually, springs can be manufactured using any available material. Although, an ideal spring material should possess low elasticity modulus, E, and higher values of yield point and ultimate strength, so that maximum energy can be stored by spring component. Automotive industries prefer ASTM, DIN or BS specifications for manufacturing spring using various materials. Plain carbon steels, copper based alloys, high nickel steels, alloy steels, and stainless steels are materials chosen for majority of spring applications. The very common spring material, SAE 5160 carbon steel, was selected for analysis in this research. This material possesses high yield strength, and the chemical composition is described below [114]:

Table 3.2: Chemical Composition of SAE 5160 Carbon Steel.

Carbon	Chrome	Manganese	Molybdenum	Silicon	Vanadium
0.56 - 0.64%	0.70 - 0.90%	0.75 - 1.00%	0.15 - 0.25%	0.15 - 0.30%	0.15%

The carbon composition of spring steel can be categorised as low to medium carbon steel having availability of carbon ranging from 0.3 % to 0.6 %. Fatigue testing of heat treated samples can be used for obtaining the cyclic properties of spring material i.e. SAE 5160 carbon steel.

3.3.2 Hexahedron Meshing Element

The 3D solid hexahedron element, as shown in Fig. 3.7 (left) and Fig. 3.8, comprises of six faces and eight nodes. Each node of element has three translational DOFs, and there are in total of twenty-four DOFs in one solid element. Figure 3.7 (right) is the meshed model of spring having six active coils as shown in Fig. 3.6 (c). The meshed model is comprising of 27058 hexahedron finite elements, and 110130 nodes.
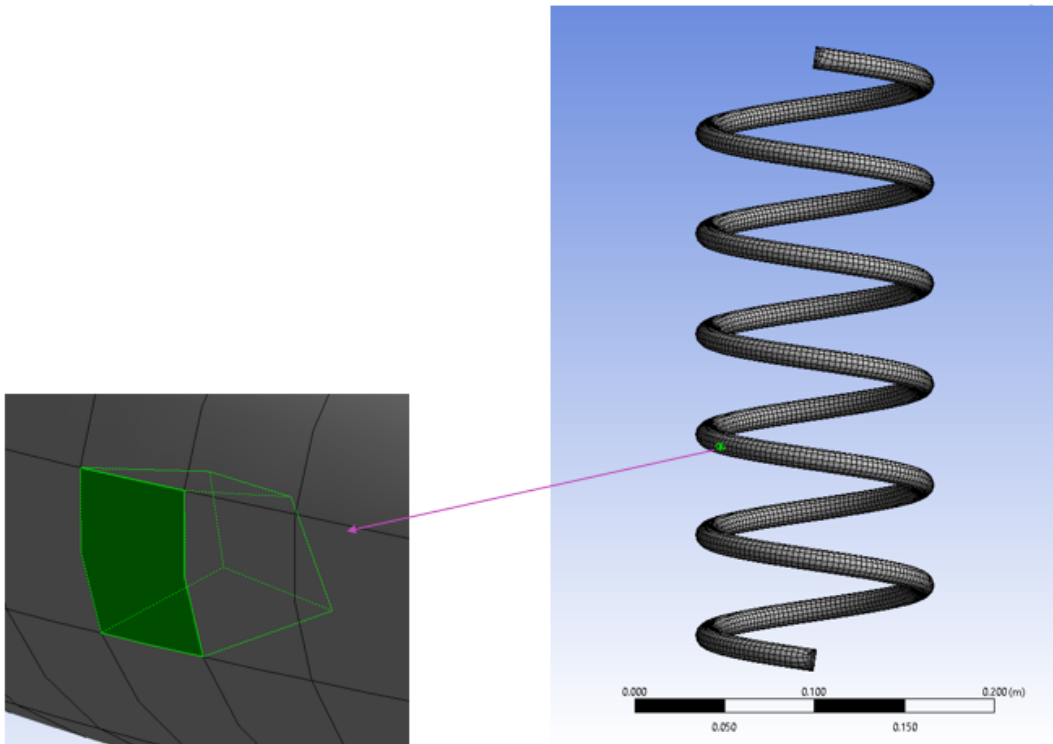
Figure 3.7: 8-Nodal Hexahedron Meshed Element.
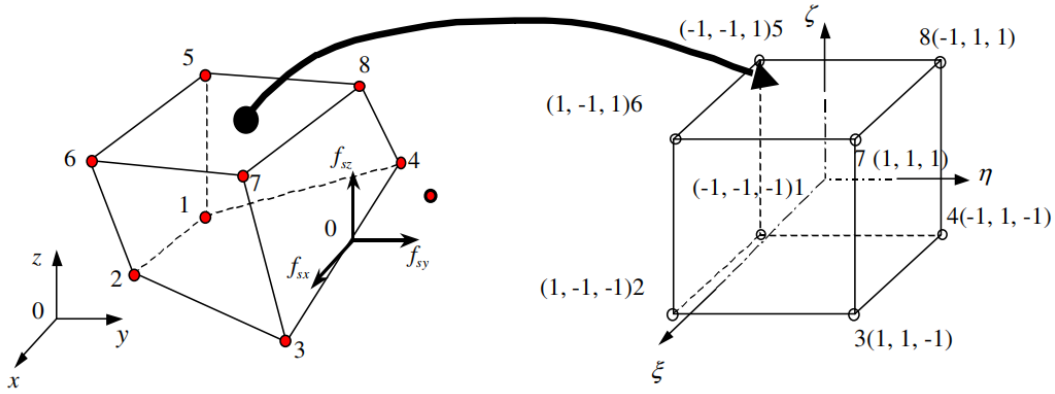
Figure 3.8: Mapping of Hexahedron in Two Coordinate Systems.
Source: Liu and Quek [140]

This 3D element is capable of deforming in all three directions in space. The shape functions defined in natural coordinate system, (ξ, η, ζ), are described below [140]:

$$N_i = \frac{1}{8} \left(1 + \xi\xi_i\right)\left(1 + \eta\eta_i\right)\left(1 + \zeta\zeta_i\right) \tag{3.27}$$

here N_i is shape function of node, i, and (ξ_i, η_i, ζ_i) represent natural nodal coordinates. The matrix of shape function, $\mathbf{N}$ (3×24), for a hexahedron element is represented as

$$\mathbf{N} = \begin{bmatrix} \mathbf{N}_1 & \mathbf{N}_2 & \mathbf{N}_3 & \mathbf{N}_4 & \mathbf{N}_5 & \mathbf{N}_6 & \mathbf{N}_7 & \mathbf{N}_8 \end{bmatrix} \tag{3.28}$$

where each sub-matrix, $\mathbf{N}_i$ (3×3), is described as

$$\mathbf{N}_i = \begin{bmatrix} N_i & 0 & 0 \\ 0 & N_i & 0 \\ 0 & 0 & N_i \end{bmatrix} \quad (i = 1, 2, .., 8) \tag{3.29}$$

For hexahedron shaped 3D finite element, the strain matrix, $\mathbf{B}$ (6×24), is expressed as

$$\mathbf{B} = \begin{bmatrix} \mathbf{B}_1 & \mathbf{B}_2 & \mathbf{B}_3 & \mathbf{B}_4 & \mathbf{B}_5 & \mathbf{B}_6 & \mathbf{B}_7 & \mathbf{B}_8 \end{bmatrix} \tag{3.30}$$

where each sub-matrix, $\mathbf{B}_i$ (6×3), is given as

$$\mathbf{B}_i = \mathbf{L}\mathbf{N}_i = \begin{bmatrix} \partial/\partial x & 0 & 0 \\ 0 & \partial/\partial y & 0 \\ 0 & 0 & \partial/\partial z \\ 0 & \partial/\partial z & \partial/\partial y \\ \partial/\partial z & 0 & \partial/\partial x \\ \partial/\partial y & \partial/\partial x & 0 \end{bmatrix} \begin{bmatrix} N_i & 0 & 0 \\ 0 & N_i & 0 \\ 0 & 0 & N_i \end{bmatrix} \tag{3.31}$$

here $\mathbf{L}$ (6×3) is the differential operator. The Jacobian matrix, $\mathbf{J}$ (3×3), considers the interpolation between the two coordinate systems, (x, y, z) and (ξ, η, ζ), is defined below:

$$\mathbf{J} = \begin{bmatrix} \frac{\partial x}{\partial \xi} & \frac{\partial y}{\partial \xi} & \frac{\partial z}{\partial \xi} \\ \frac{\partial x}{\partial \eta} & \frac{\partial y}{\partial \eta} & \frac{\partial z}{\partial \eta} \\ \frac{\partial x}{\partial \zeta} & \frac{\partial y}{\partial \zeta} & \frac{\partial z}{\partial \zeta} \end{bmatrix} \tag{3.32}$$

The stiffness matrix, $\mathbf{k}_e$ (24×24), for 3D solid hexahedron element is computed using the strain matrix, $\mathbf{B}$, is expressed as [140]

$$\mathbf{k}_e = \int_{V_e} \mathbf{B}^T \mathbf{c} \mathbf{B} \, \mathrm{d}V = \int_{-1}^{+1} \int_{-1}^{+1} \int_{-1}^{+1} \mathbf{B}^T \mathbf{c} \mathbf{B} \det[\mathbf{J}] \, \mathrm{d}\xi \mathrm{d}\eta \mathrm{d}\zeta \tag{3.33}$$

here $\mathbf{c}$ is a symmetric matrix of material constants. For an isotropic spring material, $\mathbf{c}$ (6×6)

matrix, is explicitly written as

$$\mathbf{c} = \begin{bmatrix} c_{11} & c_{12} & c_{12} & 0 & 0 & 0 \\ c_{12} & c_{11} & c_{12} & 0 & 0 & 0 \\ c_{12} & c_{12} & c_{11} & 0 & 0 & 0 \\ 0 & 0 & 0 & (c_{11} - c_{12})/2 & 0 & 0 \\ 0 & 0 & 0 & 0 & (c_{11} - c_{12})/2 & 0 \\ 0 & 0 & 0 & 0 & 0 & (c_{11} - c_{12})/2 \end{bmatrix} \tag{3.34}$$

here c_{ij} represents material constants, and they are expressed as

$$\begin{aligned} c_{11} &= \frac{E(1 - \nu)}{(1 - 2\nu)(1 + \nu)} \\ c_{12} &= \frac{E\nu}{(1 - 2\nu)(1 + \nu)} \end{aligned} \tag{3.35}$$

where E and ν represent modulus of elasticity, and Poisson's ratio. The mass or inertia matrix, $\mathbf{m}_e$ (24×24), is obtained using shape function matrix, $\mathbf{N}$, which is given as [140]

$$\mathbf{m}_e = \int_{V_e} \rho \mathbf{N}^T \mathbf{N} \, dV = \int_{-1}^{+1} \int_{-1}^{+1} \int_{-1}^{+1} \rho \mathbf{N}^T \mathbf{N} \det[\mathbf{J}] \, d\xi d\eta d\zeta \tag{3.36}$$

here ρ is density of spring material. For hexahedron element, displacement vector, $\{\mathbf{U}_e\}$ (3×1), is interpolated using the shape functions, $\mathbf{N}$, is described as

$$\{\mathbf{U}_e\} = \mathbf{N}\{\mathbf{d}_e\} \tag{3.37}$$

56

where nodal displacement vector, $\{\mathbf{d}_e\}$ (24×1), takes the form

$$\{\mathbf{d}_e\} = \begin{Bmatrix} \mathbf{d}_1 \\ \mathbf{d}_2 \\ \mathbf{d}_3 \\ \mathbf{d}_4 \\ \mathbf{d}_5 \\ \mathbf{d}_6 \\ \mathbf{d}_7 \\ \mathbf{d}_8 \end{Bmatrix} \tag{3.38}$$

here $\{\mathbf{d}_i\}$ (3×1) is displacement vector at node, i, represented as

$$\{\mathbf{d}_i\} = \begin{Bmatrix} u_i \\ v_i \\ w_i \end{Bmatrix} \quad (i = 1, 2, .., 8) \tag{3.39}$$

here u_i, v_i and w_i are nodal displacements along x, y and z axes respectively. Similarly, the nodal displacement vector, $\{\mathbf{U}_i\}$ (3×1), is evaluated as mentioned below:

$$\{\mathbf{U}_i\} = \mathbf{N}_i\{\mathbf{d}_i\} \tag{3.40}$$

here $\mathbf{N}_i$ is matrix of nodal shape function as obtained from Eq. 3.29.

Considering a 3D finite element, the corresponding vector of strain components for a given element, $\{\boldsymbol{\epsilon}_e\}$ (6×1), is evaluated as

$$\{\boldsymbol{\epsilon}_e\} = \mathbf{L}\{\mathbf{U}_e\} = \mathbf{L}\mathbf{N}\{\mathbf{d}_e\} = \mathbf{B}\{\mathbf{d}_e\} \tag{3.41}$$

Similarly, the nodal strain vector for ith node, $\{\boldsymbol{\epsilon}_i\}$ (6×1), is described below:

$$\{\boldsymbol{\epsilon}_i\} = \mathbf{L}\{\mathbf{U}_i\} = \mathbf{L}\mathbf{N}_i\{\mathbf{d}_i\} = \mathbf{B}_i\{\mathbf{d}_i\} \tag{3.42}$$

where $\mathbf{N}_i$ is matrix of nodal shape function, $\mathbf{B}_i$ is nodal strain matrix, and $\{\mathbf{d}_i\}$ represents displacement vector at node, i.

Using the constitutive equation, termed as Hooke's law, the stress components for a 3D hexahedron element, $\{\boldsymbol{\sigma}_e\}$ (6×1), is written in following matrix form:

$$\{\boldsymbol{\sigma}_e\} = \mathbf{c}\{\boldsymbol{\epsilon}_e\} \tag{3.43}$$

and the corresponding nodal stress vector for ith node, $\{\boldsymbol{\sigma}_i\}$ (6×1), is evaluated as

$$\{\boldsymbol{\sigma}_i\} = \mathbf{c}\{\boldsymbol{\epsilon}_i\} \tag{3.44}$$

here $\mathbf{c}$ (6×6) is material constants matrix, obtained from Eq. 3.34.

3.3.3   Boundary Conditions

There are two boundary conditions applied on finite element model of coil spring. The bottom cross-section of model is fixed, while the top cross-section is allowed to displace only along the vertical axial direction. The two DOFs of all nodes on the top cross-section are constrained, and for bottom cross-section nodes, all the three DOFs of each node are constrained. The six active coils between bottom and top end cross-sections are free to deform in any direction. Mathematically, the boundary conditions are expressed below.

For nodes on bottom cross-section:

$$u_i = v_i = w_i = 0 \qquad (3.45)$$

For nodes on top cross-section:

$$u_i = w_i = 0 \qquad (3.46)$$

here u_i, v_i and w_i are displacements of node, i, along x, y and z axes respectively.

3.3.4 Formulation of Finite Element Method

This chapter describes formulation of finite element equations in local, and global coordinate systems. Solving the equations result in evaluating displacement of nodes, and subsequently the stress induced at nodes of finite element. The obtained governing equations of motion are further utilised for static, and frequency response analyses of helical coil spring, which are discussed below in later sections.

3.3.4.1 Finite Element Formulation in Local Coordinate System

The finite element equation for an element is formulated after constructing the shape functions. The strain-displacement matrix, **B**, provides the strain information in element, using the element nodal displacements. After determination of strain matrix, the element stiffness matrix, $\mathbf{k}_e$, and mass matrix of element, $\mathbf{m}_e$, are obtained. Liu and Quek [140] derived the

59

FEM equation of motion for an element, expressed as

$$\mathbf{m}_e\{\ddot{\mathbf{d}}_e\} + \mathbf{k}_e\{\mathbf{d}_e\} = \{\mathbf{f}_e\} \tag{3.47}$$

where $\{\mathbf{d}_e\}$ is displacement vector for nodes of an element, and $\{\mathbf{f}_e\}$ is element force vector acting on the nodes of element.

3.3.4.2 Obtaining the Global Finite Element Equation

A coordinate transformation is required to convert elemental equation from local coordinate system to global system. The transformation is performed using the transformation matrix, $\mathbf{T}$, and mathematically represented as

$$\begin{aligned} \{\mathbf{d}_e\} &= \mathbf{T}\{\mathbf{D}_e\} \\ \{\mathbf{f}_e\} &= \mathbf{T}\{\mathbf{F}_e\} \end{aligned} \tag{3.48}$$

After substituting the above expressions, the obtained finite element equation based on the global coordinate system, is mentioned below [140]:

$$\mathbf{M}_e\{\ddot{\mathbf{D}}_e\} + \mathbf{K}_e\{\mathbf{D}_e\} = \{\mathbf{F}_e\} \tag{3.49}$$

here

$$\begin{aligned} \mathbf{K}_e &= \mathbf{T}^T\mathbf{k}_e\mathbf{T} \\ \mathbf{M}_e &= \mathbf{T}^T\mathbf{m}_e\mathbf{T} \\ \{\mathbf{F}_e\} &= \mathbf{T}^T\{\mathbf{f}_e\} \end{aligned} \tag{3.50}$$

60

The FE equations generated from all elements in global coordinate system, are assembled together to obtain the global Finite Element equation of system, which is

$$\mathbf{M}\{\ddot{\mathbf{D}}\} + \mathbf{K}\{\mathbf{D}\} = \{\mathbf{F}\} \tag{3.51}$$

where $\mathbf{K}$ and $\mathbf{M}$ represent global stiffness and mass matrices, $\{\mathbf{D}\}$ is global vector of nodal displacements, and $\{\mathbf{F}\}$ represents global vector comprising of equivalent nodal force vectors.

3.3.5   Static Analysis of Coil Spring

During static analysis, term involving the global mass matrix, $\mathbf{M}$, from Eq. 3.51 is not considered. The representation of static system of equations, is expressed as

$$\mathbf{K}\{\mathbf{D}\} = \{\mathbf{F}\} \tag{3.52}$$

There are multiple techniques to solve for global static displacement vector of all elements, $\{\mathbf{D}\}$, in above Eq. 3.52. The Gauss elimination or LU decomposition methods are commonly used for solving the above system of equations.

For further analysis, the global displacement vector of element, $\{\mathbf{D}_e\}$, is extracted from $\{\mathbf{D}\}$, which is utilised to evaluate the local displacement vector of element, $\{\mathbf{d}_e\}$, using the mathematical relation expressed in Eq. 3.48. The local nodal displacement vector, $\{\mathbf{d}_i\}$, is obtained from $\{\mathbf{d}_e\}$, which is used to generate the nodal strain vector, $\{\boldsymbol{\epsilon}_i\}$, using Eq. 3.42. Finally, the static analysis provides the nodal stress, $\{\boldsymbol{\sigma}_i\}$, calculated using $\{\boldsymbol{\epsilon}_i\}$ from the expression in Eq. 3.44.

3.3.6 Frequency Response Analysis of Coil Spring

This section discuss the governing equations of motion, that are required to be solved during the modal and harmonic analyses of helical spring. The modal analysis is performed for obtaining the modal natural frequencies, and corresponding modal shapes, considering the undamped system and free vibration analysis. The modal results are prerequisites to conduct the harmonic analysis on helical spring model. Mathematical formulations of modal and harmonic analyses are discussed in subsequent sections.

3.3.6.1 Modal Analysis

The general linear equation of motion is expressed by Eq. 3.51. Modal analysis is performed on deformed configuration obtained from static analysis. The technique considers the system to be free from external force i.e. it becomes the case $\{\mathbf{F}\} = \{0\}$, also called free vibration analysis [140]. Under undamped and free vibration, Eq. 3.51 transforms into system equation expressed as

$$\mathbf{M}\{\ddot{\mathbf{D}}\} + \mathbf{K}\{\mathbf{D}\} = \{0\} \tag{3.53}$$

For a harmonic motion, Eq. 3.53 is reduced to an eigen value problem, Eq. 3.54 [141].

$$[\mathbf{K} - \lambda\mathbf{M}]\{\phi\} = \{0\} \tag{3.54}$$

where λ is equal to ω^2. In order to obtain non trivial solution for $\{\phi\}$, determinant of below

matrix should be equated to zero, which is mathematically represented as

$$\det\left[\mathbf{K} - \lambda\mathbf{M}\right] = 0 \tag{3.55}$$

The solution of above polynomial equation are called as eigen values, λ_i, which are related to natural frequencies of component, ω_i, corresponding to ith mode. After substituting the eigen value, λ_i, in Eq. 3.54, a set of algebraic equations are obtained, which are mathematically expressed as mentioned below [140]:

$$\left[\mathbf{K} - \lambda_i\mathbf{M}\right]\{\phi_i\} = \{0\} \tag{3.56}$$

Solving these algebraic equations result in eigen vector, $\{\phi_i\}$, corresponding to the eigen value, λ_i. Mathematically, eigen vectors are utilised to generate the displacement fields, and an eigen vector, $\{\phi_i\}$, constructs the shape of component vibrating in ith mode.

3.3.6.2   Harmonic Analysis of Coil Spring

Harmonic analysis determines response of suspension spring to the excitation at various frequencies. The governing equations of motion, with damping effects into consideration, are represented as

$$\mathbf{M}\{\ddot{\mathbf{D}}\} + \mathbf{C}\{\dot{\mathbf{D}}\} + \mathbf{K}\{\mathbf{D}\} = \{\mathbf{F}\} \tag{3.57}$$

here $\{\mathbf{D}\}$ is global vector of displacements of all elements, and $\mathbf{C}$ is damping coefficients matrix. The damping coefficient matrix, $\mathbf{C}$, is obtained as [142, 143]

$$\mathbf{C} = c_K\mathbf{K} + c_M\mathbf{M} \tag{3.58}$$

here c_K and c_M represent damping coefficients.

Considering harmonic analysis, the force vector, $\{\mathbf{F}\}$, and the displacement vector, $\{\mathbf{D}\}$, in Eq. 3.57 are expressed as

$$\begin{aligned}
\{\mathbf{F}\} &= \{\mathbf{F}_0\}e^{i\Omega t} \\
\{\mathbf{D}\} &= \{\mathbf{D}_0\}e^{i\Omega t}
\end{aligned} \tag{3.59}$$

here Ω is the excitation frequency. Taking into consideration, the sinusoidal behavior of excitation force, and corresponding displacement of node, after substituting the parameters from Eq. 3.59 in Eq. 3.57, the harmonic equations of motion takes the form:

$$\left(-\Omega^2 \mathbf{M} + i\Omega \mathbf{C} + \mathbf{K}\right)\{\mathbf{D}_0\} = \{\mathbf{F}_0\} \tag{3.60}$$

The solution of the above harmonic equations, Eq. 3.60, results in the global time-independent displacement vector, $\{\mathbf{D}_0\}$. Further, the global displacement vector of element, $\{\mathbf{D}_e\}$, is extracted from $\{\mathbf{D}_0\}$, which is utilised in evaluation of local displacement vector of element, $\{\mathbf{d}_e\}$, using the mathematical expression in Eq. 3.48. The local nodal displacement vector, $\{\mathbf{d}_i\}$, is obtained from $\{\mathbf{d}_e\}$, which generates the nodal strain vector, $\{\boldsymbol{\epsilon}_i\}$, using Eq. 3.42. Using constitutive model and the nodal strain components, $\{\boldsymbol{\epsilon}_i\}$, in Eq. 3.44, the nodal stress vector, $\{\boldsymbol{\sigma}_i\}$, is obtained based on the harmonic response analysis.

3.4 Summary

The FEA methodologies deployed in this research have been discussed in this chapter. All the necessary mathematical equations are expressed to evaluate the displacement, and stress

obtained from static and harmonic analyses. The techniques were employed to attain the objectives of analysing the fatigue life, and durability of helical suspension spring. Utilising the mathematical formulations from this Chapter 3, the subsequent Chapter 4 presents the obtained results that demonstrate the objectives of this research. The validation of discussed results provide confirmation to the originality of the analysis performed under this thesis.

Chapter 4

RESULTS AND DISCUSSION

4.1 Introduction

The results are presented in this chapter in accordance with the requirement of durability assessment. The FEA was performed by simulating the spring model under actual loading conditions. The analysis has been conducted through dual step process. The former step obtains the static equilibrium position of spring from the static linear analysis. In the later step, modal and frequency response analyses are performed on the deformed configuration about the static equilibrium position of coil spring model. The results led to identification of critical location in the helical spring, and estimation of fatigue life along with durability analysis of suspension spring component.

4.2 Determination of Durability Characteristics

The static linear analysis determines the static equilibrium position, and von-Mises stress distribution in coil spring. The modal analysis is performed about the static equilibrium position, for evaluating natural frequencies, and corresponding modal shapes. Further, the harmonic analysis generates stress amplitude of vibration in coil spring. Subsequently, the frequency response of stress amplitude is used for fatigue life evaluation of spring model.

4.2.1   Static Mean Stress Analysis

The static displacement, $\{\mathbf{D}\}$, is evaluated using Eq. 3.52 by substituting $\mathbf{K}$ with $\mathbf{K}_0$, and $\{\mathbf{F}\}$ is obtained from weight of vehicle. Here $\mathbf{K}_0$ represents the global stiffness matrix of spring model generated from static undeformed length, L_f (Fig. 2.10). The boundary conditions applied for static analysis are expressed by Eq. 3.45 and Eq. 3.46. The plot below describes the total static displacement of 3D spring model.
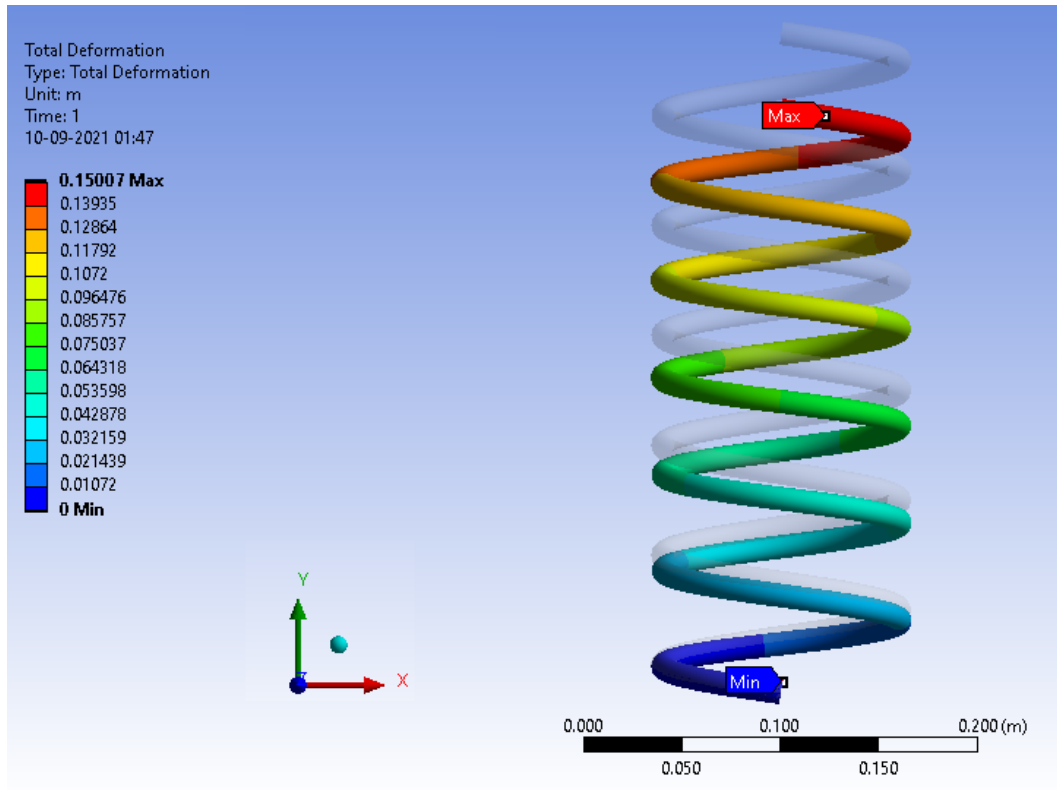
Figure 4.1: Total Static Displacement of Coil Spring Model.

The maximum spring displacement obtained from static analysis is 15.007 cm, which is used to evaluate the spring stiffness, K, from Hooke's law, Eq. 2.2. The deformed length of spring, L_a, from static analysis is the static equilibrium position of the deformed configuration. Further, the static nodal displacement, $\{\mathbf{d}_i\}$, is obtained from $\{\mathbf{D}\}$, which

67

is utilized to obtain the nodal strain vector, $\{\epsilon_i\}$, using Eq. 3.42, and that subsequently is used to generate the nodal stress vector, $\{\sigma_i\}$, by solving Eq. 3.44. The plot highlighting the von-Mises stress distribution in spring CAD model is shown below:
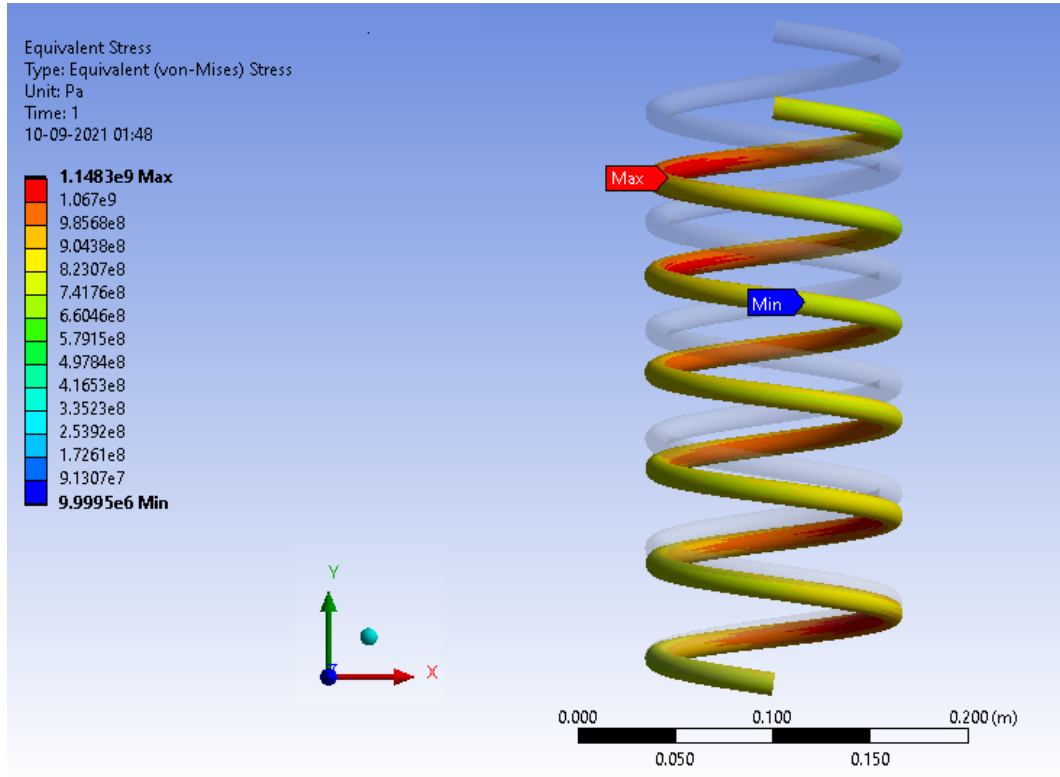
Figure 4.2: von-Mises Stress Distribution in Coil Spring Model.

The maximum von-Mises stress value comes out to be 1148.3 MPa, which is used as the static mean stress at equilibrium position, σ_m, for the fatigue life assessment using Eq. 2.21, that is discussed below in later section. After performing the static linear analysis on initial Lagrange's configuration, the outcome of FEA simulation resulted in the indication of region corresponding to critical maximum von-Mises stress induced in spring model. The von-Mises stress contour was obtained, and location of maximum critical von-Mises stress in coil spring model was observed to occur along the periphery of inner curvature of spring.

The developed CAD model of helical coil spring was evaluated through FEA, and

analytical calculation using Eq. 3.4. Difference was observed in between the analytically calculated, and FEA obtained spring stiffness values. Consequently, analysis of the deviation in results was required for assuring the validation of the 3-dimensional CAD model of helical spring. The assessment of obtained stiffness values of spring is expressed below:

Table 4.1: Assessment of Spring Stiffness Values.

FEA simulation	Analytical calculation	Deviation
19610.8 N/m	19903.8 N/m	**1.47%**

The deviation of 1.47% was observed in the values of spring stiffness. The variation of FEA simulation and analytical experimental results was acceptable upto 10% [144]. Hence, the designed model of helical coil spring was validated for performing the stress evaluation, modal, and harmonic analyses leading to more precise prediction of fatigue life.

4.2.2 Modal Analysis and Modal Shapes

During the initial stage of this research work, FEA was performed on automotive suspension spring model for obtaining distribution of von-Mises stress contour. Initiation of crack takes place at the critical stress location which directly leads to failure due to fatigue. In case of uni-directional loading, the critical von-Mises stress location is observed at inner region of coil spring. The deformed configuration of helical spring model, initially meshed using 3D hexahedron (hex) shaped finite elements, is deployed for performing modal analysis. The practical frequency range of 0 Hz to 200 Hz is considered during modal analysis evaluations.

The static mean stress, σ_m, is pre-applied on CAD spring model, to be utilized for modal analysis calculations. The modal analysis about static equilibrium position is performed using Ansys Workbench™ software package on the deformed configuration as obtained from static linear analysis. The modal resonance frequencies, and corresponding

modal shapes are obtained using Eq. 3.56 by substituting $\mathbf{K}$ with $\mathbf{K}_S$, where $\mathbf{K}_S$ represents the global stiffness matrix evaluated from spring model having static deformed length, L_a (Fig. 2.10). The first 20 modal natural frequencies evaluated in between 0 Hz to 200 Hz are

Table 4.2: Modal Natural Frequencies between 0 Hz to 200 Hz.

Mode, i	Frequency (Hz)	Mode, i	Frequency (Hz)
1	24.24	11	141.66
2	53.02	12	150.82
3	53.59	13	153.58
4	54.94	14	155.39
5	71.71	15	162.07
6	95.97	16	171.63
7	98.40	17	180.38
8	105.27	18	180.62
9	115.42	19	186.05
10	139.54	20	197.70

And the corresponding modal shapes for first 6 natural frequencies are shown as

(Mode 1)　　(Mode 2)　　(Mode 3)

(Mode 4)　　(Mode 5)　　(Mode 6)
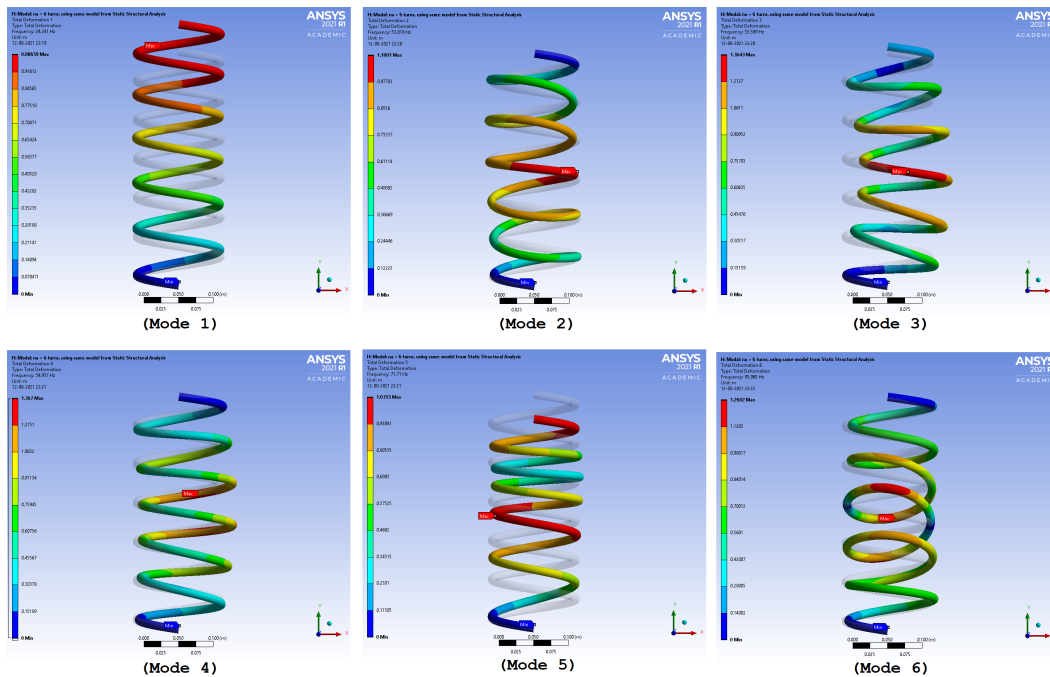
Figure 4.3: Deformed (Color) and Undeformed (Grey) Modal Shapes for First 6 Modes.

Figure 4.3 above describes the 6 modal shapes for both the deformed (color) and undeformed (grey) configurations of spring model. The same boundary conditions are applied for the static and modal analyses, as expressed by Eq. 3.45 and Eq. 3.46.

4.2.3 Frequency Response of Stress Amplitude

The frequency dependent displacement vector, $\{\mathbf{D}_0\}$, under harmonic analysis is obtained by solving Eq. 3.60. Further, the harmonic nodal displacement, $\{\mathbf{d}_i\}$, is obtained from $\{\mathbf{D}_0\}$, which is used to derive the nodal strain vector, $\{\boldsymbol{\epsilon}_i\}$, using Eq. 3.42, and subsequently the nodal stress vector, $\{\boldsymbol{\sigma}_i\}$, is evaluated from Eq. 3.44. The frequency response of stress amplitude considers maximum von-Mises stress in the spring model at a particular frequency value. The frequency response data obtained from harmonic analysis of helical spring model, over practical frequency range of 0 Hz to 200 Hz, is described in the two plots below:
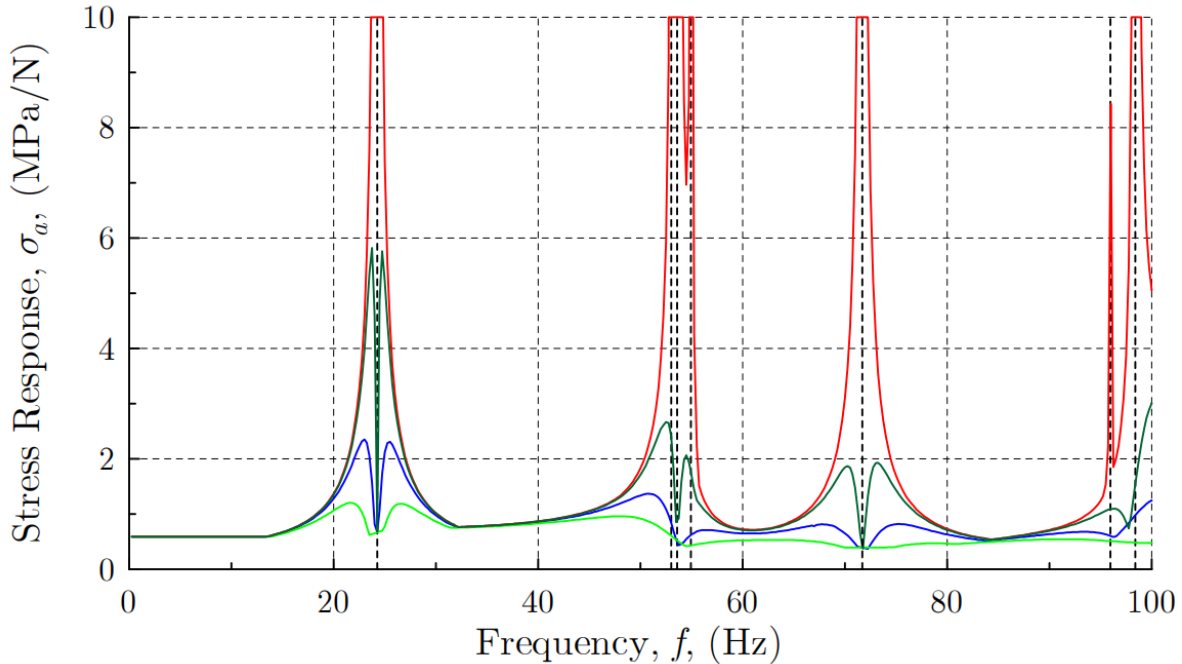
Figure 4.4: Plot of Stress Response and Frequency, from 0 Hz to 100 Hz.
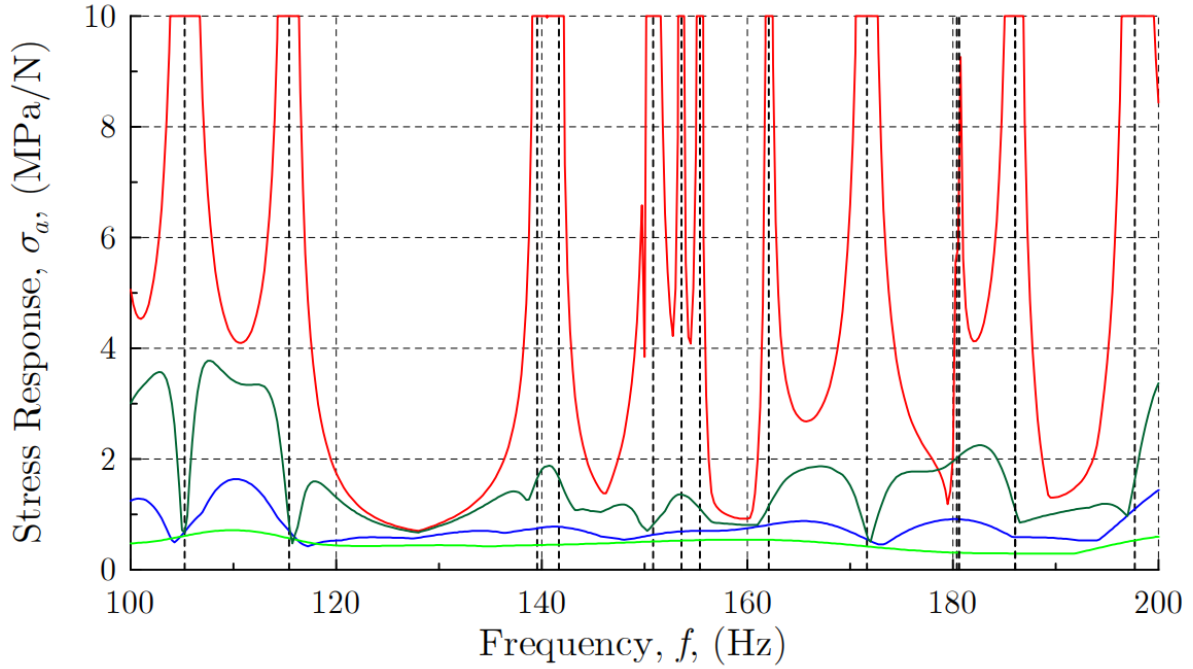
Figure 4.5: Plot of Stress Response and Frequency, from 100 Hz to 200 Hz.

The 20 modal natural frequencies as observed on the above two plots, Fig. 4.4 and Fig. 4.5, are represented using vertical dotted lines. The vertical axis on the curve has unit of MPa/N for maximum von-Mises stress response, σ_a. The stress response attains peak value near the resonance modal frequencies. The spring damping of 0% (**red**), 2% (**dark-green**), 5% (**blue**), and 10% (**light-green**) are represented on the two plots. Damping in the suspension is inversely proportional to the stress response, σ_a. In other words, with the increase in damping value of coil spring, the corresponding stress response value keeps on decreasing. However, the damping value of spring can not go beyond a certain value in order to obtain a smooth and stable ride. The value of optimum damping for spring is desired while designing the components of vehicle suspension system.

In this research, the range of frequency chosen for fatigue assessment of vehicle suspension spring is from 0 Hz to 200 Hz, and considering a passenger car, analysing for

frequency up to 200 Hz is quite practical. However, natural frequency of overall vehicle suspension system can be obtained in between 1 Hz to 3 Hz. Considering the engine component of vehicle, the resonance frequency comes in between 20 Hz to 200 Hz having the range of engine speed from 600 rpm to 6000 rpm [145]. For the investigation of fatigue life behavior of suspension spring, performing the frequency responses analysis along with durability assessment are required.

4.2.4 Durability Assessment

The cyclic and mechanical properties of suspension spring material, SAE 5160 carbon steel, have been tabulated below [146]:

Table 4.3: Cyclic and Mechanical Properties of SAE 5160 Carbon Steel.

Material Properties	Values
Density, ρ	7850 kg/m^3
Modulus of elasticity, E	207 GPa
Poisson's ratio, ν	0.3
Tensile yield strength	1487 MPa
Ultimate tensile strength	1584 MPa
Fatigue strength coefficient, σ'_f	2063 MPa
Cyclic strength coefficient	2432 MPa
Fatigue strength exponent, b	-0.08
Fatigue ductility exponent	-1.05
Fatigue ductility coefficient	9.56
Cyclic strain hardening exponent	0.13

Considering the above spring material properties, the description of parameters utilised for evaluation of fatigue life, N_f, of coil spring, using Eq. 2.21, are mentioned in Table 4.4. The mean stress, σ_m, is obtained from static linear analysis of coil spring. For the spring material, the **Endurance Limit** is reached, when fatigue life, N_f, is greater than 10^8 cycles (Fig. 2.15), while the **Stress Failure** occurs with fatigue life, N_f, lower than 10^4 cycles.

Table 4.4: Various Parameters Used for Fatigue Life Estimation.

Parameter	Expression/Value
System damping, ζ	10%
Amplitude of road surface, y_0	1 cm, 2 cm
Velocity of vehicle, V	60, 80, 100, 120 km/h
Wavelength of road surface, L	25, 50, 75, 100, 200, 500 cm
Excitation frequency, f	V/L
Force applied in spring	F_s
Mean stress applied on spring, σ_m	1148.3 MPa
Spring material	SAE 5160 carbon steel
Fatigue strength coefficient, σ'_f	2063 MPa
Fatigue strength exponent, b	-0.08
Fatigue life	N_f
Endurance Limit	$N_f > 10^8$ cycles
Stress Failure	$N_f < 10^4$ cycles

The durability assessment of spring having excitation amplitude, y_0 (Fig. 3.3), of 1 cm is

L (cm)	V (km/h)	f (Hz)	F_s (N)	Spring damping = 2%			Spring damping = 5%		
				σ_a^* (MPa/N)	$\sigma_a = \sigma_a^* \times F_s$ (MPa)	N_f (cycles)	σ_a^* (MPa/N)	$\sigma_a = \sigma_a^* \times F_s$ (MPa)	N_f (cycles)
25	60	66.67	196.18	1.06	207.95	55010600	0.78	153.02	Endurance Limit
	80	88.89	196.15	0.66	129.46	Endurance Limit	0.62	121.61	Endurance Limit
	100	111.11	196.13	3.34	655.07	Stress Failure	1.60	313.81	321110
	120	133.33	196.13	1.07	209.86	49074500	0.70	137.29	Endurance Limit
50	60	33.33	196.40	0.77	151.23	Endurance Limit	0.76	149.26	Endurance Limit
	80	44.44	196.27	1.02	200.20	88466200	0.98	192.35	Endurance Limit
	100	55.56	196.21	1.25	245.26	6991400	0.68	133.42	Endurance Limit
	120	66.67	196.18	1.06	207.95	55010600	0.78	153.02	Endurance Limit
75	60	22.22	196.75	2.70	531.23	Stress Failure	1.99	391.53	20200
	80	29.63	196.47	1.05	206.29	60797300	1.03	202.36	77318800
	100	37.04	196.34	0.81	159.04	Endurance Limit	0.79	155.11	Endurance Limit
	120	44.44	196.27	1.02	200.20	88466200	0.98	192.35	Endurance Limit
100	60	16.67	197.26	0.80	157.81	Endurance Limit	0.77	151.89	Endurance Limit
	80	22.22	196.75	2.70	531.23	Stress Failure	1.99	391.53	20200
	100	27.78	196.52	1.59	312.47	338770	1.37	269.23	2179530
	120	33.33	196.40	0.77	151.23	Endurance Limit	0.76	149.26	Endurance Limit
200	60	8.33	200.80	0.59	118.47	Endurance Limit	0.58	116.46	Endurance Limit
	80	11.11	198.72	0.59	117.21	Endurance Limit	0.59	117.20	Endurance Limit
	100	13.89	197.77	0.62	121.77	Endurance Limit	0.61	120.92	Endurance Limit
	120	16.67	197.26	0.80	158.54	Endurance Limit	0.77	151.77	Endurance Limit
500	60	3.33	229.51	0.59	134.96	Endurance Limit	0.59	134.95	Endurance Limit
	80	4.44	213.63	0.59	125.67	Endurance Limit	0.59	125.66	Endurance Limit
	100	5.56	206.98	0.59	121.81	Endurance Limit	0.59	121.80	Endurance Limit
	120	6.67	203.53	0.59	119.85	Endurance Limit	0.59	119.83	Endurance Limit

Figure 4.6: Fatigue Life Assessment I of Coil Spring.

The fatigue life, N_f, is evaluated using Eq. 2.21, and the static mean stress, σ_m, is maximum von-Mises stress obtained from static linear analysis of spring model. Considering the fatigue life assessment as described in Fig. 4.6, with the increase in value of spring damping from 2% to 5%, the induced stress, σ_a, decreases, resulting in increase of fatigue life, N_f. There are 20 natural resonance frequencies from modal analysis, between 0 Hz to 200 Hz, as listed in Table 4.2. The magnitude of stress, σ_a, rises significantly as the excitation frequency, f approaches any of the modal natural frequencies, ω_i. Multiple **Endurance Limit** scenarios are observed in Fig. 4.6 which signifies vehicle traveling on smooth road surface conditions.

The durability assessment of vehicle suspension spring travelling through a road surface model as shown in Fig. 3.3, and having excitation amplitude value, y_0, of 2 cm is

				Spring damping = 2%			Spring damping = 5%		
L (cm)	V (km/h)	f (Hz)	F_s (N)	$\sigma_a{}^*$ (MPa/N)	$\sigma_a = \sigma_a{}^* \times F_s$ (MPa)	N_f (cycles)	$\sigma_a{}^*$ (MPa/N)	$\sigma_a = \sigma_a{}^* \times F_s$ (MPa)	N_f (cycles)
25	60	66.67	392.36	1.06	415.90	Stress Failure	0.78	306.04	439250
	80	88.89	392.30	0.66	258.92	3551610	0.62	243.23	7759410
	100	111.11	392.27	3.34	1310.18	Stress Failure	1.60	627.63	Stress Failure
	120	133.33	392.25	1.07	419.71	Stress Failure	0.70	274.58	1704870
50	60	33.33	392.79	0.77	302.45	509113	0.76	298.52	599485
	80	44.44	392.54	1.02	400.39	15272	0.98	384.67	25181
	100	55.56	392.42	1.25	490.53	Stress Failure	0.68	266.85	2436140
	120	66.67	392.36	1.06	415.90	Stress Failure	0.78	306.04	439250
75	60	22.22	393.51	2.70	1062.48	Stress Failure	1.99	783.09	Stress Failure
	80	29.63	392.94	1.05	412.59	10495	1.03	404.73	13347
	100	37.04	392.68	0.81	318.07	271273	0.79	310.22	370792
	120	44.44	392.54	1.02	400.39	15272	0.98	384.69	25181
100	60	16.67	394.52	0.80	315.62	298859	0.77	303.78	481900
	80	22.22	393.51	2.70	1062.48	Stress Failure	1.99	783.09	Stress Failure
	100	27.78	393.04	1.59	624.93	Stress Failure	1.37	538.47	Stress Failure
	120	33.33	392.79	0.77	302.45	509113	0.76	298.52	599485
200	60	8.33	401.60	0.59	236.94	10761700	0.58	232.93	13325500
	80	11.11	397.44	0.59	234.42	12303300	0.59	234.40	12316400
	100	13.89	395.54	0.62	243.54	7636840	0.61	241.83	8338280
	120	16.67	394.52	0.80	317.09	281972	0.77	303.55	486532
500	60	3.33	459.02	0.59	269.92	2111520	0.59	269.90	2113090
	80	4.44	427.25	0.59	251.34	5149040	0.59	251.32	5153660
	100	5.56	413.96	0.59	243.61	7607120	0.59	243.60	7611800
	120	6.67	407.07	0.59	239.69	9316200	0.59	239.66	9330790

Figure 4.7: Fatigue Life Assessment II of Coil Spring.

There are multiple **Stress Failure** scenarios observed in Fig. 4.7 that signifies the vehicle is traveling on rough road surface conditions. When excitation frequency, f, is exactly equal to any modal natural frequency, ω_i, the induced stress, σ_a, reaches infinite magnitude to hit the resonance condition. Considering a particular value of wavelength of road surface, L, as the velocity of vehicle, V, gradually increases from 60 km/h to 120 km/h, the applied force in spring, F_s, reduces in magnitude. For the same value of excitation frequency, f, the road surface having amplitude of 1 cm (Fig. 4.6) has comparatively lower stress, σ_a, and larger fatigue life, N_f, and therefore is comparatively smoother than road surface amplitude of 2 cm (Fig. 4.7).

4.3 Summary

The results corresponding to static linear analysis, modal analysis, and harmonic analysis have been expressed and discussed in this chapter. The various analyses performed were in accordance with the defined objectives for this research. The techniques utilized for evaluation of vehicle body frequency, vibration, and spring fatigue life has made important contribution in the novelty of research. Overall, proposed technique utilized in this research can provide significant contribution in designing of vehicle suspension spring, considering the fatigue life behavior and improving the ride characteristics of automobile. The design procedure of suspension spring is time consuming process along with fatigue life estimation, and vehicle ride performance evaluation corresponding to stiffness value of spring, and subsequent damping of suspension system. The proposed analysis in the thesis work aims to ease this complicated process of spring design, for improving the vibration fatigue life.

Chapter 5

CONCLUSION

5.1   Conclusion

The aim to this research is to propose an approach to predict the fatigue life, and assess the durability of suspension coil spring using inputs as body response of vehicle, road surface excitation, and vehicle ride characteristics. The technique utilized in this thesis focuses on simplifying the vehicle suspension spring design, using estimation of fatigue life behavior. The execution of this research generated optimum characteristics of durability for prediction of fatigue life, and vibration properties of spring having sustainable precision as well as replicability and reliability. The current study can estimate the fatigue life of spring, and the vibration behavior corresponding to the stiffness parameter of helical coil spring.

5.2   Research Contribution

The design stages of vehicle suspension need significant number of hours and considerable human efforts. This research provides a novel approach for estimation of relationships to diminish the required time and efforts. Using the body frequency of vehicle system, road surface induced vibrations, and vehicle ride characteristics as inputs for analysis, fatigue life as spring can be estimated with sustainable accuracy. In other words, the road induced

vibrations can be evaluated by using body frequency of vehicle, and fatigue life of spring as inputs. The obtained results in this research can contribute in these three areas of design of vehicle suspension, ride analysis of automobiles, and structural durability analysis. This study could bridge the gap existing in between these three domains of mechanical engineering. The research outcome could be beneficial for automotive industries in addressing vehicle suspension component prototyping issues, saving money and time. Furthermore, researchers from academia, and automotive industries could enhance the understanding of analysing effect of road induced vibration on fatigue life of vehicle suspension component.

5.3 Future Research

This current research has developed an innovative approach for durability assessment of vehicle suspension spring, contributing to the various branches of mechanical engineering. There are some futuristic research areas, utilising the current work, listed below:

1. Considering practical applications, the suspension springs are subjected to multi-axial road surface loadings. The current work could be extended to the deformation of spring along multiple axes, and evaluating the induced vibrations in lateral and longitudinal directions.

2. The linear and single DOF quarter car model was analysed for extracting the responses of spring and the vehicle. A non-linear and multiple DOFs model could provide more accurate results for durability assessment of automotive spring.

3. The developed road model could be expanded to generate an innovative tool for analysing more complex road surface conditions. The road surface could be modeled

using probabilistic distribution of harmonic wavelength, L, that directly influences the excitation frequency, f.

4. This current performed study could develop a novel and robust procedure for the probabilistic fatigue life prediction of automotive mechanical components, including the suspension spring.

Bibliography

[1] L.-K. Song, C.-W. Fei, J. Wen, and G.-C. Bai, "Multi-objective reliability-based design optimization approach of complex structure with multi-failure modes," *Aerospace Science and Technology*, vol. 64, pp. 52–62, 2017.

[2] I. Coutinho, J. Landre Jr, P. A. Magalhães, M. Caiafa, and M. Toledo, "Rear suspension damper support virtual durability and load reconstruction," 2016.

[3] J.-H. Zhu, W.-H. Zhang, and L. Xia, "Topology optimization in aircraft and aerospace structures design," *Archives of Computational Methods in Engineering*, vol. 23, no. 4, pp. 595–622, 2016.

[4] X. Ye, Y. Su, and J. Han, "A state-of-the-art review on fatigue life assessment of steel bridges," *Mathematical Problems in Engineering*, vol. 2014, 2014.

[5] A. Varvani-Farahani, M. Sharma, and M. Kianoush, "Fatigue damage analysis and life assessment under variable amplitude loading conditions," *Materials Science and Engineering: A*, vol. 403, no. 1-2, pp. 42–47, 2005.

[6] P. Gupta, C. Lacerda, V. S. Patil, D. Biswal, P. Wattamwar, J. Zach Hilt, and T. D. Dziubla, "Degradation of poly (β-amino ester) gels in alcohols through transesterification: Method to conjugate drugs to polymer matrices," *Journal of Polymer Science Part A: Polymer Chemistry*, vol. 55, no. 12, pp. 2019–2026, 2017.

[7] N. E. Dowling, "Mean stress effects in stress-life and strain-life fatigue," tech. rep., SAE Technical Paper, 2004.

[8] F. Liu, S. Zhou, C. Xia, D. Zeng, and T. Shi, "Optimization of fatigue life distribution model and establishment of probabilistic s–n curves for a 165 ksi grade super high strength drill pipe steel," *Journal of Petroleum Science and Engineering*, vol. 145, pp. 527–532, 2016.

[9] R. Fragoudakis, S. Karditsas, G. Savaidis, and N. Michailidis, "The effect of heat and surface treatment on the fatigue behaviour of 56sicr7 spring steel," *Procedia Engineering*, vol. 74, pp. 309–312, 2014.

[10] S.-I. Moon, I.-J. Cho, and D. Yoon, "Fatigue life evaluation of mechanical components using vibration fatigue analysis technique," *Journal of mechanical science and technology*, vol. 25, no. 3, pp. 631–637, 2011.

[11] V. S. Patil, T. D. Dziubla, and D. S. Kalika, "Static and dynamic properties of biodegradable poly (antioxidant β-amino ester) networks based on incorporation of curcumin multiacrylate," *Polymer*, vol. 75, pp. 88–96, 2015.

[12] K. C. Panda, "Dealing with noise and vibration in automotive industry," *Procedia Engineering*, vol. 144, pp. 1167–1174, 2016.

[13] D. S. Paraforos, H. W. Griepentrog, and S. G. Vougioukas, "Country road and field surface profiles acquisition, modelling and synthetic realisation for evaluating fatigue life of agricultural machinery," *Journal of Terramechanics*, vol. 63, pp. 1–12, 2016.

[14] E. Ganjian, M. Khorami, and A. A. Maghsoudi, "Scrap-tyre-rubber replacement for aggregate and filler in concrete," *Construction and building materials*, vol. 23, no. 5, pp. 1828–1836, 2009.

[15] Y.-S. Huang, C.-D. Huang, and J.-W. Ho, "A customized two-dimensional extended

warranty with preventive maintenance," *European Journal of Operational Research*, vol. 257, no. 3, pp. 971–978, 2017.

[16] M. Saraf *et al.*, "Measurement of road profile and study it's effect on vehicle durability and ride," tech. rep., SAE Technical Paper, 2009.

[17] B. Pyttel, I. Brunner, B. Kaiser, C. Berger, and M. Mahendran, "Fatigue behaviour of helical compression springs at a very high number of cycles–investigation of various influences," *International journal of fatigue*, vol. 60, pp. 101–109, 2014.

[18] Y. Zhu, Y. Wang, and Y. Huang, "Failure analysis of a helical compression spring for a heavy vehicle's suspension system," *Case Studies in Engineering Failure Analysis*, vol. 2, no. 2, pp. 169–173, 2014.

[19] A. C. Mitra and N. Banerjee, "A labview-based data acquisition system in a quarter car test rig to optimize vehicle suspension system," in *Intelligent Computing and Applications*, pp. 593–601, Springer, 2015.

[20] A. Thite, "Development of a refined quarter car model for the analysis of discomfort due to vibration," *Advances in Acoustics and Vibration*, vol. 2012, 2012.

[21] Y. S. Saurabh, S. Kumar, K. K. Jain, S. K. Behera, D. Gandhi, S. Raghavendra, and K. Kalita, "Design of suspension system for formula student race car," *Procedia Engineering*, vol. 144, pp. 1138–1149, 2016.

[22] X. Shao, N. Xu, and X. Liu, "Investigation and application on the vertical vibration models of the seated human body," *Automotive Innovation*, vol. 1, no. 3, pp. 263–271, 2018.

[23] C. Scheiblegger, N. Roy, P. E. Pfeffer, and A. Hillis, "Modeling hydro mounts in

vehicles for durability load analyses, ride comfort and vehicle dynamics simulation," in *Advanced Vehicle Control AVEC'16*, pp. 703–710, CRC Press, 2016.

[24] S. Gu, "Application of finite element method in mechanical design of automotive parts," in *IOP conference series: materials science and engineering*, vol. 231, p. 012180, IOP Publishing, 2017.

[25] S. M. H. Rizvi, M. Abid, A. Q. Khan, S. G. Satti, and J. Latif, "H∞ control of 8 degrees of freedom vehicle active suspension system," *Journal of King Saud University-Engineering Sciences*, vol. 30, no. 2, pp. 161–169, 2018.

[26] W. S. Aboud, S. M. Haris, and Y. Yaacob, "Advances in the control of mechatronic suspension systems," *Journal of Zhejiang University SCIENCE C*, vol. 15, no. 10, pp. 848–860, 2014.

[27] R. N. Jazar, " quarter car model," in *Vehicle Dynamics*, pp. 985–1026, Springer, 2014.

[28] A. Purushotham, "Comparative simulation studies on macpherson suspension system," *International Journal of Modern Engineering Research (IJMER)*, vol. 3, no. 3, pp. 1377–1381, 2013.

[29] H. Yarmohamadi and V. Berbyuk, "Kinematic and dynamic analysis of a heavy truck with individual front suspension," *Vehicle system dynamics*, vol. 51, no. 6, pp. 877–905, 2013.

[30] S. A. A. Naeem and P. Jagtap, "Analysis of upper control arm for finding optimized model using fea and experimentation," *Imperial Journal of Interdisciplinary Research (IJIR) Vol-3, Issue-3*, 2017.

[31] M. Blundell and D. Harty, *Multibody systems approach to vehicle dynamics.* Elsevier, 2004.

[32] S. Uberti, M. Gadola, D. Chindamo, M. Romano, and F. Galli, "Design of a double wishbone front suspension for an orchard–vineyard tractor: Kinematic analysis," *Journal of Terramechanics*, vol. 57, pp. 23–39, 2015.

[33] A. Bhatt, "Kinematic analysis of formula sae suspension," 2010.

[34] A. A. Sequeira, R. K. Singh, and G. K. Shetti, "Comparative analysis of helical steel springs with composite springs using finite element method," *Journal of Mechanical Engineering and Automation*, vol. 6, no. 5A, pp. 63–70, 2016.

[35] E. Kreyszig, K. Stroud, and G. Stephenson, "Advanced engineering mathematics," *Integration*, vol. 9, p. 4, 2008.

[36] A. Choube, "Finite element analysis of helical spring in mono suspension system," *International Journal of Engineering Science and Computing*, vol. 6, no. 5, pp. 4947–4951, 2016.

[37] J. C. Dixon, *The shock absorber handbook.* John Wiley & Sons, 2008.

[38] D. Schramm, M. Hiller, and R. Bardini, "Vehicle dynamics," *Modeling and Simulation. Berlin, Heidelberg*, vol. 151, 2014.

[39] V. Cossalter, A. Doria, R. Pegoraro, and L. Trombetta, "On the non-linear behaviour of motorcycle shock absorbers," *Proceedings of the Institution of Mechanical Engineers, Part D: Journal of Automobile Engineering*, vol. 224, no. 1, pp. 15–27, 2010.

[40] G. Koch, E. Pellegrini, S. Spirk, and B. Lohmann, "Design and modeling of a quarter-vehicle test rig for active suspension control," tech. rep., Lehrstuhl für Regelungstechnik, 2010.

[41] M. Mahmoodi-Kaleibar, I. Javanshir, K. Asadi, A. Afkar, and A. Paykani, "Optimization of suspension system of off-road vehicle for vehicle performance improvement," *Journal of central south university*, vol. 20, no. 4, pp. 902–910, 2013.

[42] D.-H. Kim, D.-H. Choi, and H.-S. Kim, "Design optimization of a carbon fiber reinforced composite automotive lower arm," *Composites Part B: Engineering*, vol. 58, pp. 400–407, 2014.

[43] C. Kavitha, S. A. Shankar, B. Ashok, S. D. Ashok, H. Ahmed, and M. U. Kaisan, "Adaptive suspension strategy for a double wishbone suspension through camber and toe optimization," *Engineering science and technology, an international journal*, vol. 21, no. 1, pp. 149–158, 2018.

[44] K. V. Reddy, M. Kodati, K. Chatra, and S. Bandyopadhyay, "A comprehensive kinematic analysis of the double wishbone and macpherson strut suspension systems," *Mechanism and Machine Theory*, vol. 105, pp. 441–470, 2016.

[45] P. R. Childs, *Mechanical design engineering handbook*. Butterworth-Heinemann, 2013.

[46] A. Gandomi, "Structural optimization using interior search algorithm," *Iranian Journal of Structural Engineering*, vol. 2, 2016.

[47] G. S. Rathore and U. K. Joshi, "Fatigue stress analysis of helical compression spring: a review," *International Journal of Emerging Trends in Engineering and Development*, vol. 2, no. 3, pp. 512–520, 2013.

[48] S. N. Khurd, P. P. Kulkarni, S. D. Katekar, and A. M. Chavan, "Analysis of two wheeler suspension spring by using fea for different materials," *International Research Journal of Engineering and Technology*, vol. 3, no. 01, pp. 2395–0056, 2016.

[49] E. Evin, M. Tomáš, J. Kmec, S. Németh, B. Katalinic, and E. Wessely, "The deformation properties of high strength steel sheets for auto-body components," *Procedia Engineering*, vol. 69, pp. 758–767, 2014.

[50] Y.-L. Lee, M. E. Barkey, and H.-T. Kang, *Metal fatigue analysis handbook: practical problem-solving techniques for computer-aided engineering*. Elsevier, 2011.

[51] Y. Upadhyaya and B. Sridhara, "Fatigue life prediction: a continuum damage mechanics and fracture mechanics approach," *Materials & Design*, vol. 35, pp. 220–224, 2012.

[52] M. Aygül, M. Al-Emrani, and S. Urushadze, "Modelling and fatigue life assessment of orthotropic bridge deck details using fem," *International Journal of Fatigue*, vol. 40, pp. 129–142, 2012.

[53] S. A. Kaoua, K. Taibi, N. Benghanem, K. Azouaoui, and M. Azzaz, "Numerical modelling of twin helical spring under tensile loading," *Applied Mathematical Modelling*, vol. 35, no. 3, pp. 1378–1387, 2011.

[54] N. Lavanya, P. S. Rao, and M. P. Reddy, "Design and analysis of a suspension coil spring for automotive vehicle," *International Journal of Engineering Research and Applications*, vol. 4, no. 9, pp. 151–157, 2014.

[55] T. Coppola, L. Cortese, and P. Folgarait, "The effect of stress invariants on ductile fracture limit in steels," *Engineering Fracture Mechanics*, vol. 76, no. 9, pp. 1288–1302, 2009.

[56] G. Vukelic and M. Brcic, "Failure analysis of a motor vehicle coil spring," *Procedia Structural Integrity*, vol. 2, pp. 2944–2950, 2016.

[57] D. V. Shevale and N. Khaire, "Review on failure analysis of helical compression spring," *International Journal of Science, Engineering and Technology Research*, vol. 5, no. 4, pp. 892–898, 2016.

[58] J.-J. Thomas, A. Bignonnet, and G. Perroud, "Fatigue design and experimentations with variable amplitude loadings in the automotive industry," in *Fatigue Testing and Analysis Under Variable Amplitude Loading Conditions*, ASTM International, 2005.

[59] B.-y. He, S.-x. Wang, and F. Gao, "Failure analysis of an automobile damper spring tower," *Engineering Failure Analysis*, vol. 17, no. 2, pp. 498–505, 2010.

[60] J. Karthik, K. Chaitanya, and C. T. Sasanka, "Fatigue life prediction of a parabolic spring under non-constant amplitude proportional loading using finite element method," *International Journal of Advanced Science and Technology*, vol. 46, pp. 143–156, 2012.

[61] K. Zakaria, S. Abdullah, M. Ghazali, M. Nuawi, S. Beden, and Z. Nopiah, "Fatigue strain signal behaviour and damage assessment of an engine mount bracket," 2014.

[62] A. de Jesus and A. da Silva, "Identification of the net effective strain-life model for a puddle iron from the portuguese fão riveted road bridge," *Procedia Engineering*, vol. 2, no. 1, pp. 1181–1190, 2010.

[63] L. Capponi, M. Česnik, J. Slavič, F. Cianetti, and M. Boltežar, "Non-stationarity index in vibration fatigue: Theoretical and experimental research," *International Journal of Fatigue*, vol. 104, pp. 221–230, 2017.

[64] M. Karlsson, *Load modelling for fatigue assessment of vehicles–a statistical approach.* Chalmers Tekniska Hogskola (Sweden), 2007.

[65] F. Chaari, M. S. Abbes, F. V. Rueda, A. F. del RINCON, and M. Haddar, "Analysis of planetary gear transmission in non-stationary operations," *Frontiers of Mechanical Engineering*, vol. 8, no. 1, pp. 88–94, 2013.

[66] A. Lennie, S. Abdullah, Z. Nopiah, and M. Baharin, "Behavioural investigation of fatigue time series using the statistical approach," *Journal of applied Sciences*, vol. 10, no. 16, pp. 1714–1722, 2010.

[67] Y. Gao, "Fatigue stress concentration sensitivity and stress ratio effect of a 40crni2si2mova steel," *Materials Letters*, vol. 186, pp. 235–238, 2017.

[68] H. Kovacı, A. F. Yetim, Ö. Baran, and A. Çelik, "Fatigue crack growth behavior of dlc coated aisi 4140 steel under constant and variable amplitude loading conditions," *Surface and Coatings Technology*, vol. 304, pp. 316–324, 2016.

[69] T. Mottitschka, G. Pusch, H. Biermann, L. Zybell, and M. Kuna, "Influence of overloads on the fatigue crack growth in nodular cast iron: experiments and numerical simulation," *Procedia Engineering*, vol. 2, no. 1, pp. 1557–1567, 2010.

[70] M. J. Doré and S. J. Maddox, "Accelerated fatigue crack growth in 6082 t651 aluminium alloy subjected to periodic underloads," *Procedia Engineering*, vol. 66, pp. 313–322, 2013.

[71] M. L. Facchinetti, "Fatigue damage of materials and structures assessed by wöhler and gassner frameworks: recent insights about load spectra for the automotive," *Procedia engineering*, vol. 213, pp. 117–125, 2018.

[72] V. Anes, J. Caxias, M. Freitas, and L. Reis, "Fatigue damage assessment under random and variable amplitude multiaxial loading conditions in structural steels," *International Journal of Fatigue*, vol. 100, pp. 591–601, 2017.

[73] A. Kulkarni, S. A. Ranjha, and A. Kapoor, "Fatigue analysis of a suspension for an in-wheel electric vehicle," *Engineering Failure Analysis*, vol. 68, pp. 150–158, 2016.

[74] J. Korhonen, J. Kuoppala, M. Väntänen, J. Vaara, M. Turunen, P. Kämäräinen, J. Laine, A. Silvonen, and T. Frondelius, "Qt steel high cycle fatigue testing with ultrasonic," *Rakenteiden Mekaniikka*, vol. 50, no. 3, pp. 304–308, 2017.

[75] M. A. Tafti, *Experimental High Cycle Fatigue Testing and Shape Optimization of Turbine Blades.* PhD thesis, 2013.

[76] G. Pantazopoulos, A. Vazdirvanidis, A. Rikos, and A. Toulfatzis, "Analysis of abnormal fatigue failure of forklift forks," *Case Studies in Engineering Failure Analysis*, vol. 2, no. 1, pp. 9–14, 2014.

[77] K. R. Lyathakula and F.-G. Yuan, "Demonstration of prognostics health monitoring (phm) in adhesive lap joints using simulated studies," *Structural Health Monitoring 2019*, 2019.

[78] K. R. Lyathakula and F.-G. Yuan, "Fatigue damage prognosis of adhesively bonded joints via a surrogate model," in *Sensors and Smart Structures Technologies for Civil, Mechanical, and Aerospace Systems 2021*, vol. 11591, p. 115910K, International Society for Optics and Photonics, 2021.

[79] R. Jiang and D. Murthy, "A study of weibull shape parameter: Properties and significance," *Reliability Engineering & System Safety*, vol. 96, no. 12, pp. 1619–1626, 2011.

[80] K. Takahashi, T. Amano, K. Ando, and F. Takahashi, "Improvement of fatigue limit by shot peening for high-strength steel containing a crack-like surface defect," *International Journal of Structural Integrity*, 2011.

[81] C. M. Sonsino, "Course of sn-curves especially in the high-cycle fatigue regime with regard to component design and safety," *International Journal of Fatigue*, vol. 29, no. 12, pp. 2246–2258, 2007.

[82] H. A. dos Santos, F. Auricchio, and M. Conti, "Fatigue life assessment of cardiovascular balloon-expandable stents: a two-scale plasticity–damage model approach," *Journal of the mechanical behavior of biomedical materials*, vol. 15, pp. 78–92, 2012.

[83] E. Ghafoori, M. Motavalli, A. Nussbaumer, A. Herwig, G. Prinz, and M. Fontana, "Determination of minimum cfrp pre-stress levels for fatigue crack prevention in retrofitted metallic beams," *Engineering Structures*, vol. 84, pp. 29–41, 2015.

[84] G. Fajdiga and M. Sraml, "Fatigue crack initiation and propagation under cyclic contact loading," *Engineering fracture mechanics*, vol. 76, no. 9, pp. 1320–1335, 2009.

[85] A. Ince and G. Glinka, "A modification of morrow and smith–watson–topper mean stress correction models," *Fatigue & Fracture of Engineering Materials & Structures*, vol. 34, no. 11, pp. 854–867, 2011.

[86] C. R. Williams, Y.-L. Lee, and J. Rilly, "A practical method for statistical analysis of strain–life fatigue data," *International Journal of Fatigue*, vol. 25, no. 5, pp. 427–436, 2003.

[87] Y.-L. Lee, J. Pan, R. Hathaway, and M. Barkey, *Fatigue testing and analysis: theory and practice*, vol. 13. Butterworth-Heinemann, 2005.

[88] A. Runciman, D. Xu, A. R. Pelton, and R. O. Ritchie, "An equivalent strain/coffin–manson approach to multiaxial fatigue and life prediction in superelastic nitinol medical devices," *Biomaterials*, vol. 32, no. 22, pp. 4987–4993, 2011.

[89] S. Gribbin, J. Bicknell, L. Jorgensen, I. Tsukrov, and M. Knezevic, "Low cycle fatigue behavior of direct metal laser sintered inconel alloy 718," *International Journal of Fatigue*, vol. 93, pp. 156–167, 2016.

[90] Y.-C. Chiou and J.-K. Yang, "The effects of pre-deformation on the subsequent fatigue behaviors of sus 430 stainless steel in load-control," *International Journal of Solids and Structures*, vol. 49, no. 23-24, pp. 3263–3268, 2012.

[91] S. Taheri, L. Vincent, and J.-C. Le-roux, "A new model for fatigue damage accumulation of austenitic stainless steel under variable amplitude loading," *Procedia Engineering*, vol. 66, pp. 575–586, 2013.

[92] S. M. Khan, F. Benyahia, B. B. Bouiadjra, and A. Albedah, "Analysis and repair of crack growth emanating from v-notch under stepped variable fatigue loading," *Procedia Engineering*, vol. 74, pp. 151–156, 2014.

[93] M. Bruchhausen, B. Fischer, A. Ruiz, S. Gonzalez, P. Hähner, and S. Soller, "Impact of hydrogen on the high cycle fatigue behaviour of inconel 718 in asymmetric push–pull mode at room temperature," *International Journal of Fatigue*, vol. 70, pp. 137–145, 2015.

[94] J. Zhang, W. Li, H. Wang, Q. Song, L. Lu, W. Wang, and Z. Liu, "A comparison of the effects of traditional shot peening and micro-shot peening on the scuffing resistance of carburized and quenched gear steel," *Wear*, vol. 368, pp. 253–257, 2016.

[95] A. H. Ertas and F. O. Sonmez, "A parametric study on fatigue strength of spot-weld joints," *Fatigue & Fracture of Engineering Materials & Structures*, vol. 31, no. 9, pp. 766–776, 2008.

[96] W. Cui, "A state-of-the-art review on fatigue life prediction methods for metal structures," *Journal of marine science and technology*, vol. 7, no. 1, pp. 43–56, 2002.

[97] S. Abdullah, *Wavelet bump extraction (WBE) for editing variable amplitude fatigue loadings.* PhD thesis, University of Sheffield, 2005.

[98] J. E. Mottershead, "Finite elements for dynamical analysis of helical rods," *International Journal of Mechanical Sciences*, vol. 22, no. 5, pp. 267–283, 1980.

[99] L. M. Jugulkar, S. Singh, and S. M. Sawant, "Analysis of suspension with variable stiffness and variable damping force for automotive applications," *Advances in Mechanical Engineering*, vol. 8, no. 5, p. 1687814016648638, 2016.

[100] J. Dong, "Performance analysis of independent suspension coil spring," in *Journal of Physics: Conference Series*, vol. 1629, p. 012052, IOP Publishing, 2020.

[101] V. Yildirim and N. Ince, "Natural frequencies of helical springs of arbitrary shape," *Journal of Sound and Vibration*, vol. 204, no. 2, pp. 311–329, 1997.

[102] L. Becker, G. Chassie, and W. Cleghorn, "On the natural frequencies of helical compression springs," *International Journal of Mechanical Sciences*, vol. 44, no. 4, pp. 825–841, 2002.

[103] X. Xue, K. W. E. Cheng, Z. Zhang, J. Lin, D. Wang, Y. Bao, M. Wong, and N. Cheung, "Study of art of automotive active suspensions," in *2011 4th International Conference on Power Electronics Systems and Applications*, pp. 1–7, IEEE, 2011.

[104] B.-L. Choi and B.-H. Choi, "Numerical method for optimizing design variables of carbon-fiber-reinforced epoxy composite coil springs," *Composites Part B: Engineering*, vol. 82, pp. 42–49, 2015.

[105] W. Sun, D. Thompson, J. Zhou, and D. Gong, "Analysis of dynamic stiffness effect of primary suspension helical springs on railway vehicle vibration," in *Journal of Physics: Conference Series*, vol. 744, p. 012149, IOP Publishing, 2016.

[106] D. Pastorcic, G. Vukelic, and Z. Bozic, "Coil spring failure and fatigue analysis," *Engineering Failure Analysis*, vol. 99, pp. 310–318, 2019.

[107] T. Putra, N. Ali, M. Machmud, A. Bakhtiar, *et al.*, "Analysis of surface failure of coil spring in passenger vehicle suspension system," in *IOP Conference Series: Materials Science and Engineering*, vol. 523, p. 012072, IOP Publishing, 2019.

[108] C. Zhou, M. Chi, Z. Wen, X. Wu, W. Cai, L. Dai, H. Zhang, W. Qiu, X. He, and M. Li, "An investigation of abnormal vibration–induced coil spring failure in metro vehicles," *Engineering Failure Analysis*, vol. 108, p. 104238, 2020.

[109] Y. Kong, S. Abdullah, D. Schramm, M. Omar, S. Haris, and T. Bruckmann, "Mission profiling of road data measurement for coil spring fatigue life," *Measurement*, vol. 107, pp. 99–110, 2017.

[110] T. Putra, S. Abdullah, D. Schramm, M. Nuawi, and T. Bruckmann, "The need to generate realistic strain signals at an automotive coil spring for durability simulation leading to fatigue life assessment," *Mechanical Systems and Signal Processing*, vol. 94, pp. 432–447, 2017.

[111] T. E. Putra and Husaini, "Identifying strain signal characteristics of automotive suspension system subjected to road surface vibrations," in *AIP Conference Proceedings*, vol. 1983, p. 030004, AIP Publishing LLC, 2018.

[112] T. E. Putra, Husaini, and M. R. Dongoran, "Effect of vehicle speed to the fatigue life of

a coil spring based on strain-life approach," in *AIP Conference Proceedings*, vol. 2187, p. 040003, AIP Publishing LLC, 2019.

[113] T. Putra, M. Machmud, *et al.*, "Predicting the fatigue life of an automotive coil spring considering road surface roughness," *Engineering Failure Analysis*, vol. 116, p. 104722, 2020.

[114] Y. S. Kong, S. Abdullah, D. Schramm, M. Z. Omar, and S. M. Haris, "Vibration fatigue analysis of carbon steel coil spring under various road excitations," *Metals*, vol. 8, no. 8, p. 617, 2018.

[115] Y. Kong, S. Abdullah, D. Schramm, M. Omar, and S. Haris, "Development of multiple linear regression-based models for fatigue life evaluation of automotive coil springs," *Mechanical Systems and Signal Processing*, vol. 118, pp. 675–695, 2019.

[116] Y. Kong, S. Abdullah, D. Schramm, M. Omar, and S. Haris, "Optimization of spring fatigue life prediction model for vehicle ride using hybrid multi-layer perceptron artificial neural networks," *Mechanical Systems and Signal Processing*, vol. 122, pp. 597–621, 2019.

[117] C. Chin, S. Abdullah, S. Singh, A. Ariffin, and D. Schramm, "Durability assessment of suspension coil spring considering the multifractality of road excitations," *Measurement*, vol. 158, p. 107697, 2020.

[118] C. Chin, S. Abdullah, S. Singh, D. Schramm, and A. Ariffin, "Durability prediction of coil spring through multibody-dynamics-based strain generation," *Mechanical Systems and Signal Processing*, vol. 154, p. 107580, 2021.

[119] K. Park and G. H. Paulino, "Cohesive zone models: a critical review of traction-

separation relationships across fracture surfaces," *Applied Mechanics Reviews*, vol. 64, no. 6, 2011.

[120] K. R. Lyathakula and F.-G. Yuan, "A probabilistic fatigue life prediction for adhesively bonded joints via anns-based hybrid model," *International Journal of Fatigue*, p. 106352, 2021.

[121] K. R. Lyathakula and F.-G. Yuan, "Probabilistic fatigue life prediction for adhesively bonded joints via surrogate model," in *Sensors and Smart Structures Technologies for Civil, Mechanical, and Aerospace Systems 2021*, vol. 11591, p. 115910S, International Society for Optics and Photonics, 2021.

[122] S. W. Thomson and P. G. Tait, *Treatise on natural philosophy.* 1888.

[123] A. E. H. Love, *A treatise on the mathematical theory of elasticity.* Cambridge university press, 2013.

[124] W. Jiang, W. Jones, K. Wu, and T. Wang, "Non-linear and linear, static and dynamic analyses of helical springs," in *30th Structures, Structural Dynamics and Materials Conference*, p. 1200, 1989.

[125] P. Valsange, "Design of helical coil compression spring: A review," *International Journal of Engineering Research and Applications*, vol. 2, no. 6, pp. 513–522, 2012.

[126] C. Johnson, "A new approach to the design of dynamically loaded extension and compression springs," *TRANS. ASME*, vol. 71, pp. 215–226, 1949.

[127] J. Dick, "Shock-waves in helical springs," *The Engineer*, pp. 194–196, 1957.

[128] R. Geballe, "Statics and dynamics of a helical spring," *American Journal of Physics*, vol. 26, no. 5, pp. 287–290, 1958.

[129] W. H. Wittrick, "On elastic wave propagation in helical springs," *International Journal of Mechanical Sciences*, vol. 8, no. 1, pp. 25–47, 1966.

[130] Y. Kagawa, "On the dynamical properties of helical springs of finite length with small pitch," *Journal of Sound and Vibration*, vol. 8, no. 1, pp. 1–15, 1968.

[131] J. W. Phillips and G. A. Costello, "Large deflections of impacted helical springs," *the Journal of the Acoustical Society of America*, vol. 51, no. 3B, pp. 967–973, 1972.

[132] V. K. Stokes, "On the dynamic radial expansion of helical springs due to longitudinal impact," *Journal of Sound Vibration*, vol. 35, no. 1, pp. 77–99, 1974.

[133] G. Costello, "Radial expansion of impacted helical springs," 1975.

[134] S. K. Sinha and G. A. Costello, "The numerical solution of the dynamic response of helical springs.," tech. rep., ROCK ISLAND ARSENAL ILL GENERAL THOMAS J RODMAN LAB, 1976.

[135] J. Michell, "The small deformation of curves and surfaces with application to the vibrations of a helix and a circular ring," *Messenger of Mathematics*, vol. 19, pp. 68–76, 1890.

[136] A. E. H. Love, *The propagation of waves of elastic displacement along a helical wire.* 1900.

[137] Y. Lin and A. P. Pisano, "General dynamic equations of helical springs with static solution and experimental verification," 1987.

[138] W. Jiang, W. Jones, T. Wang, and K. Wu, "Free vibration of helical springs," 1991.

[139] S. Thangjitham. "Lecture Notes," ESM 5304/AOE 5034 - Mechanical And Structural Vibrations, Engineering Science and Mechanics Department, Virginia Tech, Spring 2021.

[140] G. Liu and S. Quek, "Chapter 2 - briefing on mechanics for solids and structures," in *The Finite Element Method (Second Edition)* (G. Liu and S. Quek, eds.), pp. 13–41, Oxford: Butterworth-Heinemann, second edition ed., 2014.

[141] M. Taktak, F. Dammak, S. Abid, and M. Haddar, "A finite element for dynamic analysis of a cylindrical isotropic helical spring," *Journal of Mechanics of Materials and Structures*, vol. 3, no. 4, pp. 641–658, 2008.

[142] M. Petyt, *Introduction to finite element vibration analysis.* Cambridge university press, 2010.

[143] R. Clough and J. Penzien, *Dynamics of Structures.* McGraw-Hill, 1975.

[144] Z. Zhang, W. Zhang, Z. J. Zhai, and Q. Y. Chen, "Evaluation of various turbulence models in predicting airflow and turbulence in enclosed environments by cfd: Part 2—comparison with experimental data from literature," *Hvac&R Research*, vol. 13, no. 6, pp. 871–886, 2007.

[145] Y. Yu, S. M. Peelamedu, N. G. Naganathan, and R. V. Dukkipati, "Automotive vehicle engine mounting systems: a survey," *J. Dyn. Sys., Meas., Control*, vol. 123, no. 2, pp. 186–194, 2001.

[146] A. Bhanage and K. Padmanabhan, "Static and fatigue simulation of automotive anti roll bar before dbtt," *International Journal of Applied Engineering Research*, vol. 10, no. 71, pp. 472–476, 2015.